UNIVERSITÉ DE SHERBROOKE
Faculté de Génie
Département de Génie Chimique

CFD Modeling of nanoparticle formation in a plasma synthesis reactor

Modélisation CFD de la formation de nanoparticules dans un réacteur de synthèse à plasma

Masters thesis in applied sciences
Speciality: Chemical Engineering

Norma Yadira MENDOZA GONZALEZ

Sherbrooke (Québec), Canada August 2003

Your file Votre référence
ISBN: 0-612-86669-6
Our file Notre référence
ISBN: 0-612-86669-6

Résumé

La production de particules dans des réacteurs à plasma thermique revêt un grand intérêt dans la synthèse de poudres. Une vaste gamme de poudres céramiques et métalliques a été produite en utilisant des réacteurs à plasma. La taille de ces poudres est habituellement de l'ordre du micromètre et parfois au dessous de 0.1 micromètre. Il y a un très grand intérêt pour les méthodes de production de poudres avec une taille moyenne plus petite que 0.1 micromètre. Ces poudres peuvent être utilisées pour créer des matériaux nanophasiques. L'utilisation des réacteurs à plasma thermique permet d'obtenir un taux de génération élévé et des produits de bonne qualité.

Les réactifs peuvent être injectés dans le réacteur plasma sous forme de poudres, de liquide pulvérisé ou de gaz. Si les réactifs sont injectés à l'état solide ou liquide, ils complètent leur évaporation dans la zone chaude du plasma. Les espèces gazeuses sont par la suite considérablement dissociées. Le gaz est ensuite refroidi en quittant la zone chaude. Finalement la nucléation et la croissance de particules auront lieu.

Cette étude présente la simulation de la formation de poudres métalliques dans un réacteur plasma à induction couplée (ICP). Un gaz porteur transporte les poudres métalliques dans le réacteur où elles sont transformées en gaz. Les produits sont récupérés après un procédé de refroidissement. Le modèle considère la formation de particules par nucléation et la croissance par condensation et coagulation brownienne. Le transport des particules est du à la convection, à la thermophorèse et à la diffusion brownienne. La diffusion axiale et radiale des particules a été considérée. Le code commercial de CFD(Computational Fluids Dyanmics) FLUENT© 6.0 a été utilisé pour les calculs de la mécanique des fluides et pour la croissance des particules. Ce code est couplé avec le modèle mathématique pour la dynamique des aérosols en utilisant les trois premiers moments de la distribution de tailles des particules. La simulation est appliquée à la production de poudres de fer ultrafines. Les résultats montrent le début de la formation de particules dans le réacteur et l'évolution de la taille des particules. Les champs des propriétés macroscopiques de la population d'aérosol et la contribution des différents mécanismes (nucléation, condensation, coagulation) sont analysés pour différentes combinaisons des paramètres d'opération. Une partie des résultats sont partiellement validés avec ceux de Bilodeau[1].

Abstract

Particle formation in thermal plasma reactor is of interest in the context of powder synthesis. A wide variety of ceramic and metallic powders has been synthesized in thermal plasma reactors. The size of these powders is virtually always of the order of magnitude of a micrometer, and often smaller than 0.1 μm. There is increasing interest in methods for producing powders with average particles sizes smaller than 0.1 μm which can be consolidated and sintered to create nanophase materials. Thermal plasma reactors are well suited to high-rate generation of such ultra-fine powders.

Reactants may be injected into a thermal plasma reactor in powder form, as a liquid spray, or in gaseous form. If the reactants are injected as solids or liquids then the process is usually designed to accomplish their complete vaporization in the hot plasma. Gaseous species in the hot plasma are substantially dissociated. The gas cools after flowing past the high-temperature core. Finally, particles nucleate and grow.

The present work reports on the simulation of metal powder formation in a Inductively Coupled Plasma reactor. A carrier gas transports the metal powder into the reactor in where it attains the vapor phase. The products are recovered after a quenching process. The model accounts for particle formation by nucleation and growth by condensation and brownian coagulation. Transport of particles occurs by convection, thermophoresis, and brownian diffusion. Axial and radial diffusion of particles are considered. The commercially computational fluid dynamics code FLUENT© 6.0, is used for the detailed calculation of the turbulent fluid flow and particle growth. This code is then completed with a model for aerosol dynamics using the first three moments of the particle size distribution. The simulation is applied for the production of ultrafine iron powders. The results show the onset of the particle formation in the reactor and calculating the dynamic evolution of the aggregate particle size and the specific surface area throughout the reactor. The fields of the macroscopic properties of the aerosol population and the contribution of the different mechanisms are analyzed under various conditions. The effect of different operating parameters on the properties of the powder generated is studied. Some results are partially validated by comparison with the results of Bilodeau [1].

Acknowledgments

This project was not completed solely through my own efforts. I would like to thank those who made this work possible.

It is through the guidance, patience and time of my advisor, Pierre Proulx that this work has been completed. I look forward to future work as a part of his research group.

I would like to thank my colleges Si-Wen, Fouzi, and Yann for their advices and support in my continued computation adventures!.

The friendship of all my collegues in the chemical engineering department made a nice atmosphere during all my studies.

Thanks to the CONACYT for its financial support in the first part of my master degree.

I dedicate this thesis to my family.

Norma Mendoza.

Contents

List of Figures

List of Tables

Nomenclature

Symbol	Units	Description
A_1		Condensation correction factor $(0.3626\frac{d_1}{\lambda})$
A_2		Condensation correction factor $(0.0418\frac{d_1^2}{\lambda})$
B_1		Coefficient of growth by condensation for the free molecular regime
Bi		Biot number
C_c		Cunningham correction factor
C_D		Drag coefficient
C_m,C_s,C_t		constants for the thermophoretic force
c	$kJ/(kgK)$	Specific heat
C_D	m^2/s	Diffusion coefficient of a particle of size j
d	m	Particle diameter
d_i	m	Particle diameter of a particle of size j
$f_{i,j}^r$		Approximate functions for the sum of the coagulation collisions
F_{th}	N	Thermophoretic force
G	kJ	Free energy of the embryo's formation
G_j	s^{-1}	Growth rate by vapor condensation
I	$m^{-3}s^{-1}$	Nucleation rate
i,j		Number of metallic monomers contained in a particle
k	$m^{-3}s^{-1}$	Moment order of the size distribution
K	$J/(smk)$	Thermal conductivity
Kn		Nudsen number
k_B	J/K	Boltzmann constant $(= 1.38x10^{-23})$
m_i	kg	Mass of a particle of size i
m_p	kg	Mass of the particle j
M	$kg/kmol$	Molecular mass of the gas
M_k		Moment of order k of the size distribution
n^*		Normalized concentration of particles $= n/n_0$

N_A	$1/mole$	Avogadro's number
n_i	m^{-3}	Discrete representation: j particle size concentration
Nu		Nusselt number
P	Pa	Pressure
k_B	J/K	Boltzmann constant ($= 1.38x10^{-23}$)
r_i	m	Radius of a particle of size i
R	kJ/(kmolK)	Gas constant= 8314
Re		Reynolds number
s_i	m^2	Surface of a particle of size i
S		Saturation ratio
S_c	ϕ/sm^3	Constant part source term, SIMPLER algorithm
S_c	ϕ/sm^3	Proportional part source term, SIMPLER algorithm
t	s	Time
T	K	Temperature
$\overrightarrow{u}$	m/s	Flow velocity
$\overrightarrow{u}_{th}$	m/s	Thermophoretic velocity

GREEK SYMBOLS

$\alpha(t)$	m/s^2	Accomodation coefficient
β	m^3/s	Collision coefficient between particles i and j
Γ	kg/(ms)	Diffusion coefficient, SIMPLER algorithm
∇T	K/M	Temperature Gradient
λ	m	Mean free path of the gas
$\Phi_{0,0}$	m^3/s	Mean coagulation coefficient
μ	$kg/(ms)$	Molecular viscosity
ω		Mass fraction
ρ	kg/m^3	Gas density
ρ_p	kg/m^3	Particle density
σ	N/m	Surface tension
τ		Undimensionless time of growth: $n_0\beta_{11}t$

Chapter 1

INTRODUCTION

1.1 Nanotechnology

Much attention has been paid recently to the manufacture of nanophase materials including nanoparticles; the essential starting materials for "bottom-up" nanotechnology. These materials possess novel or improved physical and chemical properties compared to the conventional coarse-grained equivalents, and therefore, they have found many different applications in diverse fields, including nano metals, nano ceramics, and nano composites [2].

Nanotechnology is concerned with development and utilization of structures and devices with organizational features at the intermediate scale between individual molecules and about 100 nm where novel properties occur as compared to bulk materials. It implies the capability to build up tailored nanostructures and devices for given functions by control at the atomic and molecular levels. Roco [3], describes the nanotechnology as an emerging enabling technology for the 21st century in addition to the already established areas of information, technology and biotechnology. This is because of the scientific convergence of physics, chemistry, biology, materials and engineering at nanoscale, and of the importance of the control of matter at nanoscale on almost all technologies.

1.1.1 Nanoparticles-essential component of nanotechnology

Nanoparticle manufacturing is an essential component of nanotechnology. The existence of this project attests to the remarkable success of nanoparticle research science. Nanoparticles have specific properties presented at the nanoparticle, nanocrystal or nanolayer level. Nanoparticles are seen either as agents of change of various phenomena and processes, or as building blocks of materials and devices with tailored characteristics.

In fact, the use of nanoparticles aims to take advantage of properties that are caused by the confinement effects, larger surface area, interactions at length scales where wave phenomena have comparable the structural features, and the possibility of generating new atomic and macromolecular structures. Important applications of nanoparticles are in dispersions and coatings, functional nanostructures, consolidated materials, biological systems and environment.

According to Roco [3], nanoparticle, crystal and nanolayer manufacturing processes aim to take the advantage of four kinds of effects:

a) Size scaling causes new physical, chemical or biological properties. Smaller particle size determines larger interfacial area, an increased number of molecules on the particle interfaces, quantum electromagnetic interactions, increased surface tension, and size confinement effects (from electronic and optic to confined crystallization and flow structures). The wavelike properties of the electrons inside matter are affected by shape an volume variations on the nanometer scale. Quantum effects become significant for organizational structures less than 50 nm, and if the particle size is less than 10 nm, these effects become significant even at room temperature;

b) New created phenomena are the result of size reduction to a value which the interaction length of physical, chemical and biological phenomena (e.g., the magnetic, laser, photonic, and heat radiation wavelengths) become comparable to the size of the particle or crystal. Examples are significant optoelectronic and magnetic properties of nanostructured materials.

c) The production of new atomic, molecular and macromolecular structures of materials is usually by different methods: chemical (chemical vapor deposition, chemical selfassembling), nanofabrication (creating nanostructures on surfaces, manipulation of three dimensional structures), or biotechnological (evolutionary approach, biotemplating, and three-dimensional molecular folding).

d) Significant increase in the degree of complexity and speed of processes in particulate systems. Time scales change because of the smaller distances and the increased spectrum of forces with intrinsically short time scales (electrostatic, magnetic, electrophoresis, radiation pressures, others).

1.2 Nanoparticles production

Nanoparticles can be synthesized using gas phase or liquid phase processes. Both methods are routinely used in industry to manufacture very large quantities of nanoparticle powders (also called "nanopowders"). Nanoparticles are attractive for the production of sintered parts because highly dense structures can be obtained at low temperature, pressure and lower sintering times. These materials are also much less prone to erosion and wear and are harder at room temperature. Examples are carbon black, iron, fumed silica, titania, etc. The economic production of these nanoparticles is still a challenge, and is being pursued by a variety of techniques in order to meet the increasing demand for these powders. Mechanical attrition, laser ablation, vapor condensation, sputtering, chemical precipitation, aerosol method and induction plasma are some of the techniques being used to produce both metallic and ceramic nanoparticles. Inductively Coupled Plasma (ICP) has received considerable attention in recent years. Furthermore, this work presents a model of nanoparticles growth using the ICP process[1].

Combustion, laser techniques, exploding wire and thermal plasma methods are examples of vapor phase generation techniques for various materials. There are other methods of production of nanoparticles as sol-gel and precipitation methods, which correspond to liquid processes.

Gas phase methods of nanoparticle synthesis have inherent advantages over wet processes because they can be used to produce purer nanoparticles. Compared to the liquid processes, these methods have the advantage of being continuous. Examples are in the production of multicomponent materials such as high-temperature superconductors.

Gas phase synthesis at high concentrations however, have disadvantages such as difficult control of size, morphology, crystalline phase, and composition which ultimately determine the properties of the nanostructured materials.

1.2.1 Production by thermal plasma

In the production of metal nanoparticles, such as iron, an inert atmosphere is needed to avoid oxidation of the metal. The thermal plasma process is a suitable choice for this purpose because of the inherent method of generation thermal plasma.

Thermal plasmas used for generation of nanoparticles are mainly arc and induction

plasma.

Induction plasma reactors allow the production of ultrafine powders of metals and ceramics of high purity. Thermal plasmas can provide the energy needed to evaporate the metal, which is injected in the form of coarse particles. A subsequent cooling of the gas containing metal vapor will produce particles with the desired specifications. These reactors are characterized by high temperatures and relatively long residence times (of the order of 10^{-1} second) compared to plasma arc torches. In Arc Plasma method, metal is melted and evaporated by using a transferred arc, then an inert gas is used to transport the evaporated metal into a tubular reactor, where it is quenched and nanoparticles are formed. Blown arc plasmas can also be used, in similar techniques to induction plasmas, when the purity of the nanoparticles is not as critical since some electrode material will eventually be found in the final product.

1.3 Modeling of nanoparticle growth

Nanoparticle growth involves nucleation and growth mechanisms. These phenomena are complex and occur rapidly in the high temperature plasma environment. For these reasons, it is difficult to characterize the particles. A mathematical model is thus a good tool to surmount these problems.

The purpose of this study is to develop a model for the formation and growth of iron nanoparticles in a turbulent regime of a plasma reactor. The model used is essentially based on the model of Bilodeau [1]. In order to solve the model, the commercial CFD software, FLUENT© 6.0 was used for the fluid mechanics and the particle dynamics calculations.

The greater possibilities of a CFD package such as FLUENT© will enable us to better describe eventual industrial reactors with all their geometric complexities.

1.4 Objectives

In this study, the final objective is to develop a model for prediction of nanoparticles growth. The following stages have to be followed:

1 Setting the fluid mechanics and particle dynamics equations which are the representation of the physics of the problem.

2 Developing a C program from the mentioned equations which is usable for the Computational Fluids Dynamics FLUENT©.

3 Carrying out the simulation using the CAD software GAMBIT© and the CFD FLUENT©

4 Analysis and validation of results with those of [1].

5 Analysis of different operating conditions: quenching gas flow rate, entrance gas flow rate, entrance metal vapor concentration and quenching design.

1.5 Contents

This thesis is made of the following chapters:

Chapter 1 is an introduction and general information about nanoparticles, including methods of production and physical properties. The role of modeling in this field is emphasized. Next, the objectives of this project are presented.

Chapter 2 is the theoretical part which gives an overview of nanoparticles production process by thermal plasma. The process by this method is first described. Next, a brief literature review of the previous works in aerosol growth modeling are presented. Then the system to be studied and phenomena controlling the process are introduced. This chapter ends with the description of the process to be modeled.

In Chapter 3 the General Dynamic Equation (which includes nucleation, condensation, coagulation, transport by convection, Brownian diffusion and thermophoresis) is transformed into a set of manageable equations using the Method of Moments. Here, the assumption is that the particle size distribution can be approximated by a lognormal size distribution everywhere in the system. Then, the assumptions and particular aspects of numerical solution linking with GAMBIT© and FLUENT© are given.

Finally, chapter 4 covers the analysis and the results of the different studies, and the general conclusion of this work. First, fluid flow fields are presented, and the analysis of the nanoparticle formation is done by considering the properties of the lognormal size distribution. Next, the influence of quenching flow rate and the concentration of

metal vapor is shown in the parametric study. This section also corresponds to the part of validation of the model, since a part of results is compared partially with those of Bilodeau [1]. At the end of the chapter,the conclusions and suggestions are presented.

Chapter 2

THEORY

2.1 Nanoparticle synthesis by inductively coupled plasma

The main advantage of the inductively coupled plasma (ICP) technology is the possibility to inject the precursor powders at the center of the plasma jet and also to synthesize in a neutral or active atmosphere. The used plasma gases are often argon, nitrogen, hydrogen or a mixture of them. Auxiliary gases can be added depending on the type of synthesis. Theses gases can be added in different levels of the plasma source to complete the reaction.

Leaving the high temperature zone of the plasma, the gases are cooled in a quenching section with very high temperature gradients. The quenching can be applied by:

a) Injecting a flow rate of a quenching gas, which produces temperature gradients of $10^8 K/s$. Common examples of quenching gas used in no reactant ICP process are Argon and Helium. This study utilizes argon as non reactant gas of quenching.

b)Contacting the hot gases with a wall cooled by water (10^5 to $10^6 K/s$)

c)Direct contact with a gas or sprayed liquid(10^6 to $10^7 K/s$).

Cooling process helps the recombination of condensable products at local temperature conditions. Normally, upon quenching, the dominant phase condenses first. It is because of the fact that nucleation rate of the solid is high compared to the other species.

Various experimental studies are mentioned for the production of metal powders Yoshida and Akashi 1981 [4], Bartmore et al. 1989 [5], Girshick et al. 1993 [6] and many others for the preparation of ceramic powders Becker et al. (1987)[7], Laflamme et al.

(1992)[8], and Soucy(1992)[9]. Figure 2.1 shows a typical diagram of the ICP process.

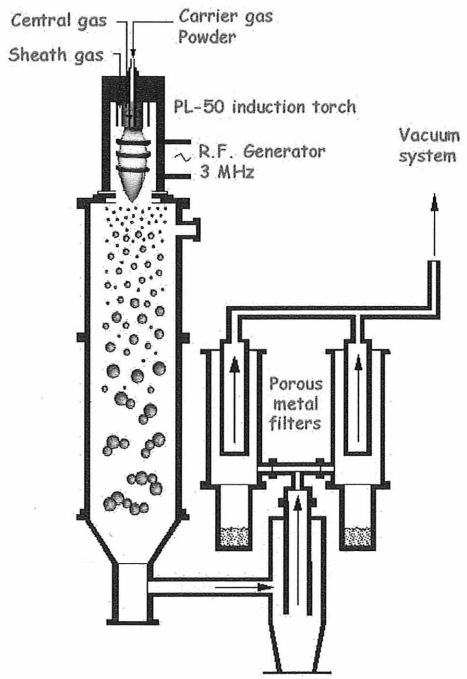

Figure 2.1: Experimental ICP plasma installation for the synthesis of nanoparticles from [10].

Nucleation and particle growth are fast phenomena and they have non uniform behavior in a plasma reactor. Modeling is a way to have a better understanding of this process. By a model it will be possible to predict and perform rates of productions. The role of modeling is to increase our capability to understand the way in which nanoparticles are formed, and has to be coupled to good experimental measurements to do so.

In the next section, some developed models in the recent 15 years are reviewed. The previous landmark work on which this study is based is also included.

2.2 Literature review

2.2.1 Modeling of nucleation and growth

Gelbard and Seinfeld (1978)[11] presented a solution for the continuous general equation by the collocation method using two different types of finite elements, line and spline

cubic interpolation. They overcame some of the difficulties of this first approach by introducing the discrete-continuous approach (Gelbar and Seinfeld 1979)[12], which solves the discrete and the continuous general equations, to describe the evolution of the particle size distribution. One of the main features of this approach is that it does not make any assumption on the shape of the particle size distribution. Other methods of solution were also developed during this time, methods such as sectional representations and discrete sectional representations for both, single and multi component aerosols (Gelbard and Seinfeld 1980; Gelbard et al. 1980)[13],[14].

Modeling of nanoparticles growth in a plasma reactor

Methods of solution discussed before were adopted into the plasma processes for the production of ultrafine particles to get a better understanding of the formation and growth of particles. A review of works concerning models for ultrafine particles synthesis is presented below.

Girshick (1988)[15] studied the formation of iron particles in a plasma reactor. A extended work was later presented [16] in a study about effect of cooling rate and metal vapor concentration on the particle size. They conclude that lower local cooling rates and higher concentrations both favor the nucleation of larger and fewer particles. Further studies on the cooling rate were conducted by Joshi et al. (1990)[17] in the production of zinc oxide in a plasma reactor. In this work, the cooling rate is determined by the quenching gas, which is injected into a Plug Flow Reactor. They found that the quenching rate can significantly influence the particle size characteristics and they proposed a gradual and controlled quenching instead of the conventionally rapid quenching.

2.2.2 Use of method of moments

Proulx and Bilodeau 1991 [18] and Bilodeau and Proulx 1992 [19] presented two-dimensional growth models in thermal plasma reactors for the particle growth along streamlines or trajectories This approach accounts for radial no uniformities but does not allow vapor and particle diffusion downstream of the nucleation line. They showed that the particle size decreases as the metal vapor concentration decreases and, as the quenching rate increases the particles size also decreases, which was in consistent with experimental results.

The model of Girshick et al. (1993) [6] considers the major growth mechanisms in the formation of ultrafine iron powders in a thermal plasma reactor. The effects of thermophoresis and radial diffusion are included in the conservation equations for moments. The model used in this work simplifies the conservation equations by neglecting the diffusion in the axial direction of the reactor. Consequently, the validity of the model is for non-recirculating flows. Conclusions yielded a good agreement with experimental data for the geometric mean diameter, however, the experimental results showed a broader size distribution. Another important contribution from this work was the development of a self consistent nucleation theory that gives similar results when using the method of moments compared to other more refined techniques (i.e. sectional representation).

Event though the method of moments has been successfully applied to one-dimensional situations, it is commonly simplified by either following the particles along streamlines (Bilodeau and Proulx 1992)[19] or by solving the parabolic simplified equations, limiting their use to non-recirculating flows. To overcome these difficulties Bilodeau [1] presented a complete model using the method of moments for two-dimensional problems, which allowed the presence of recirculating flow to be modeled. da Cruz[20] extended the model of [1] to the production of AlN and added a new nucleation rate expression (da Cruz 1997; da Cruz and Munz 2001)[21], [20]. Finally, Liu [22] studied the production of aluminum particles inside a particle generator in the laminar regime (Liu 2001). Aristizabal (2002) [23] completed this last work extending the model to account for turbulence interactions in a transferred arc plasma reactor.

2.2.3 Use of FLUENT© for numerical simulation of nanoparticle production

Kim and Pratsinis (1988)[24] developed a technical solution for simulation of particle formation and deposition by solving the Navier-Stokes equations. They used continuity; momentum, energy and mass balance equations for gas components and they also took into accounteat transfer, chemical reaction, convection, gas diffusion and SiO_2 thermophoresis of SiO_2.

Several authors have considered this principe, Stratmann and Whitby (1989) combined an existing code that uses the Simpler-algorithm (Patankar, 1980)[25] to describe coupled heat and mass transfer, fluid flow and particle dynamics. Assuming that the aerosol size distribution corresponds to a log-normal distribution, their code employs a moment method for describing the process of heterogeneous condensation in a cooled laminar tube flow.

Studies using the commercial software FLUENT© started when Johannessen (1986)[26] used it to simulate the gas temperature and velocity of alumina flame reactor. On the basis of the obtained flow, temperatures and concentrations of chemical species, the model for particle dynamics by Kruis et al. (1998) [27] was integrated along a set of characteristic trajectories.

Schild et al. (1999)[28] employs the model by Kruis et al. (1993) to describe the dynamic evolution of the particle size and number concentration by coagulation and sintering, neglecting the polydispersity of the aggregates and primary particles. In contrast to Joahannessen´s approach, here the model of Kruis et al. (1993) is completely implemented into the commercially available software package FLUENT© (version not provided).

2.3 Formation of nanoparticles-transport

External forces cause convection-like transport, due to gravitational, thermophoretic, centrifugal, electrical, magnetic, or other forces that exert a force on the particles. Because external forces cause convection-like transport, additional velocities are calculated for each of the relevant external forces, and because the effect of these processes is assumed to be additive, these velocities are added to the fluid velocity to yield the total particle velocity.

Whereas convection causes particle motion along the streamlines, external particle velocities cause particle transport that may deviate from the streamlines, including particle transport to surfaces.

Momentum phenomena exchange affecting a particle in the typical conditions of a Plasma reactor such particle drag, rarefaction effect, deviation to constant properties, Brownian motion and thermophoresis are briefly presented in this section. These phenomena represent external forces affecting the transport of particles across the boundaries. More information is giving by Rudinger (1980)[29] and Seinfeld (1986)[30].

2.3.1 Particle drag

An insulated particle in a relative movement according to a flow follows a drag force because of combining effects of viscosity and transport fluid. This force depends on size and shape, of particle, physical properties of the fluid and relative velocity. This force is expressed by the drag coefficient C_D:

$$\overrightarrow{F}_t = m_p \frac{d\overrightarrow{u}_p}{t} = C_D \frac{1}{2}\rho(\frac{1}{4}\pi d_p^2)|\overrightarrow{u} - \overrightarrow{u}_p|(\overrightarrow{u} - \overrightarrow{u}_p) \tag{2.1}$$

Coefficient C_D is a function of particle shape and Reynolds number:

$$Re = \frac{|\overrightarrow{u} - \overrightarrow{u}_p| d_p \rho}{\mu} \tag{2.2}$$

For solid spheres in the continuum regime and with constants gas properties, dependency of drag coefficient and Reynolds number is expressed as follows:

$$C_D = (\frac{24}{Re}) f(Re) \tag{2.3}$$

The Reynold functions for particles in thermal plasma conditions are given by Boulos and Gauvin (1974) [31], [32] according to the Stokes and Oseen laws:

for $Re < 0.2$ (Stokes law)

$$f(Re) = 1 \tag{2.4}$$

for $0.2 < Re < 2$ (Oseen law)

$$f(Re) = 1 + \frac{3}{16} Re \tag{2.5}$$

for $2 < Re < 20$

$$f(Re) = 1 + 0.11 Re^{0.81} \tag{2.6}$$

for $20 < Re < 500$

$$f(Re) = 1 + 0.189 Re^{0.632} \tag{2.7}$$

The flow around particles produced by ICP is often in the Stokes mode. Relative velocities are such as 10 m/s with Reynolds number of $6x10^{-2}$. Evolution of velocity as function of time is given by:

$$\overrightarrow{u}_{p,0} - \overrightarrow{u} = (\overrightarrow{u}_{p,0} - \overrightarrow{u}) \exp(-t/\tau_v) \tag{2.8}$$

$\overrightarrow{u}_{p,0}$ is the initial velocity of the particle, and the relaxation time in momentum of a spherical particle(tendency of particle for following the flow of the gas carrying) is expressed by:

$$\tau_v = \frac{\rho_p d_p^2}{18\mu} \tag{2.9}$$

2.3.2 Rarefaction effect

The rarefaction effect is observed in the plasma state. Very high temperature is not the only conditions that is conducive to plasma formation. Gas also ionizes when it is rarefied; when a gas is rarefied, free electrons virtually never encounter an ion with which it can rejoin. A phenomena related to the molecular or noncontinuum nature of gas flow at densities where $\lambda/l > 0.01$ is a rarefied gas. Where λ is the molecular mean free path and l is a characteristic dimension of the flow field.

The continuum regime supposes that the mean free path of the gas molecules is significantly lower than the size of particles. In thermal plasma reactors the mean free path of the molecules of the gas is of the order of 1 micron. Particles produced by condensation are smaller than this value, it means that the flow relative to the nanoparticles is not in the continuum regime.

The Knudsen number is defined as follows:

$$Kn = \frac{2\lambda}{d_i} \tag{2.10}$$

Where the mean free path is given by the kinetic gas theory:

$$\lambda = \frac{\mu}{0.499P(8M/RT\pi)^{1/2}} \tag{2.11}$$

The table 2.1 shows the regimes observed in function of the Knudsen number.

Slip flow and transition flow are not always distinguished from each other. This work considers the free molecule flow.

Table 2.1: TRANSFER REGIMES

Regime	*Knudsen value*
continuum	$Kn < 0.001$
slip flow	$0.001 \leq Kn < 0.1$
transition flow	$0.1 \leq Kn < 10$
free molecule flow	$Kn \geq 10$

2.3.3 Brownian diffusion

Any diminutive particle suspended in a liquid (or gas) moves chaotically under the action of collisions with surrounding molecules. The intensity of this chaotic motion is increased if temperature increases. This experimental fact was discovered by a British scientist R. Brown in 1827, and therefore is called Brownian movement.

The motion equation is expressed for a spherical particle by Seinfeld (1986)[30] who considers other phenomena as Stokes drag and the bombardment of the molecules:

$$m_i \frac{dv}{dt} = -\frac{3\pi\mu d_i}{C_c}(\vec{u}_i - \vec{u}) + m_i\alpha(t) \tag{2.12}$$

Where $\alpha(t)$ is an acceleration due to the non-continuum nature, produced by collisions between molecules of the fluid. This is a random direction force which does not generate an important displacement in the period. Nevertheless this mean square displacement is expressed by:

$$< x^2 >=< y^2 >=< z^2 >= \frac{2k_BTC_ct}{3\pi\mu d_i} \tag{2.13}$$

Particle diffusion due to Brownian motion may have significant importance for small particles flowing in the high-temperature zones downstream of a thermal plasma reactor. A balance on a diferential element leads to

$$\frac{\partial n_i}{\partial t} = \vec{\nabla} \cdot (D_i \vec{\nabla} n_i) \tag{2.14}$$

This an analogue mechanism to that of chemical species diffusion and the related coefficient associated to particles of size d is [33]:

$$D_i = \frac{k_BTC_c}{3\pi\mu d_i} = \frac{k_BT}{3\pi\mu}(1/d_i + 3.314\lambda/d_i^2) \tag{2.15}$$

2.3.4 Thermophoresis

The thermophoretic force is the force that arises from asymmetrical interactions of a particle with the surrounding gas molecules due to a temperature gradient. In simpler terms, a particle is repelled from a heated surface or attracted to a cold surface. Chemical vapor deposition processes take place in cold and hot wall reactors, with varying substrate temperatures. This array of thermal boundary conditions results in a variety of temperature gradients and thermophoretic forces on the particle. There are other forces also acting on the particles in the chemical vapor deposition environment such as inertia, Brownian motion, drag, and gravity.

The thermophoretic force caused by the temperature gradient between the heated steam and the cold reactor wall is a "natural" particle repellant (MacGibbon1999)[34], whose study shows that thermophoresis has a direct impact on the amount on the particulate deposition on the substrate due to the temperature gradients present near the substrate in a chemical vapor deposition reactor.

In a thermal plasma reactor there are strong temperature gradients (10^4K/cm)which produce deviation velocities no negligible, in the order of cm/s. Talbot (1981)[35] proposes the Brock (1962)[36] equation for the case of constant properties:

$$F_{th} = \frac{12\pi\mu^2 r_i / C_s(\frac{K}{K_p} + C_t\frac{\lambda}{r_i})}{\rho(1+3C_m\frac{\lambda}{r_i})(1+2\frac{K}{K_p}+2C_t\frac{\lambda}{r_i})}\frac{\vec{\nabla}T}{T_\infty} \tag{2.16}$$

Talbot(1981)[35] proposes 2.18, 1.14, and 1.17 as corresponding values for C_t, C_m,C_s, for the case where fluid-particles interactions are unknown. Lee(1984)[37] proposes last values for a thermal plasma case.

The dimensionless number Th, for the case of a particle with temperature equal to that of the fluid is given by:

$$Th = -(\frac{\vec{u}_{th}\rho T}{\mu\vec{\nabla}T}) \tag{2.17}$$

This dimensionless number is almost constant for $Kn >> 1$. It has been measured for the Stokes regime yielding ~ 0.5. Phanse et Pratsinis(1989)[33] suggest a constant value of Th=0.55 for particles with a size less to 1 micron.

Finally, the expression for thermophoretical velocity applied to nanoparticles in this work is:

$$\vec{u}_{th} = -\frac{0.55\mu}{\rho T}\vec{\nabla} T \tag{2.18}$$

2.4 Formation of particles-aerosol growth

The two important internal processes that modify the particle size distribution are gas-to-particle conversion and coagulation. The former refers to the transformation from the gas phase, continuous phase, to solid or liquid (particles or discrete phase). Gas-to-particle conversion includes nucleation as well as heterogeneous condensation. These phenomena: nucleation, condensation, and coagulation, in addition with the external force mechanisms can be observed in figure2.2.

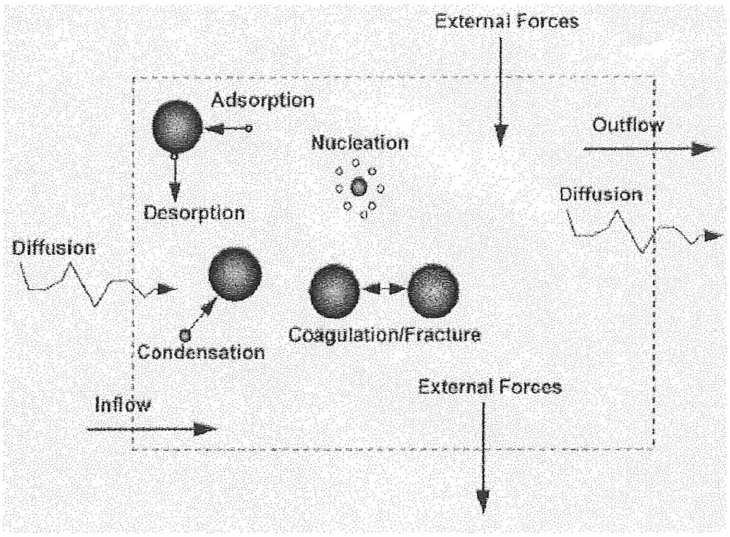

Figure 2.2: Particle processes

A detailed description of each of internal processes is given in the following section.

2.4.1 Nucleation

Nucleation is the process by which vapor condenses to form new particles. Homogeneous nucleation occurs when collision of vapor molecules alone causes the formation of new particles, and heterogeneous nucleation occurs when vapor condenses onto small particles called nuclei, to form particles that are a mixture of the nuclei and the condensed vapor.

For example, when iron is evaporated in a ICP reactor, iron vapor follows the gas flow into the particle generation reactor where the saturation ratio of iron vapor increases

due to temperature drop cause by heat transfer from the gas phase to the walls of the reactor and the injection of a quench gas. When the supersaturation can no longer be sustained, iron particles are formed by homogeneous nucleation. Small collections of iron atoms called clusters start to form only for extremely short time. Two or more atoms can form a cluster by random collisions, the size of this cluster can increase by collisions with other atoms or even with other clusters, or it can shrink in size when one atom leaves the cluster. Clusters are also formed in a supersaturated vapor, but most of them are thermodynamically unstable with respect to evaporation at the particular saturation ratio; only sufficiently large clusters are thermodynamically stable as a result of the Kelvin effect. The Kelvin effect means an increase of the vapor tension on a surface of small radius curvature. Clusters or particles are unstable with respect to evaporation unless the partial pressure around the particle is greater than the vapor pressure above the curved surface of the particle, suggesting the existence of a critical nucleus size, where smaller clusters tend to evaporate or lose atoms and shrink, and larger ones will grow.

The critical cluster size and the number of monomers contained in a particle of critical size j^* are expressed as follows:

$$d^* = \frac{4\sigma}{\rho_p R\ T\ ln\ S} \tag{2.19}$$

$$j^* = (\frac{2}{3}\frac{\theta}{lnS})^3 \tag{2.20}$$

$$\theta = \frac{\sigma s_1}{k_B T} \tag{2.21}$$

where σ is the surface tension, θ is the dimensionless surface tension and S is the supersaturation ratio, n_1 is the vapor concentration and n_s is the vapor concentration at saturation :

$$S = \frac{n_1}{n_s} \tag{2.22}$$

The *kinetic* nucleation rate expression reported by Girshick and Chiu 1990 [38] is obtained by a development similar to that to the classical expression of Becker and Döring (1935)[39]. It differs by the use of saturated vapor in equilibrium as reference for the calculation of the energy of formation of clusters. Girshick et al.[38] compare the results of the discrete model of Rao and McMurry (1989)[40], solving directly for cluster growth and evaporation from monomers, to those of a moment model using alternatively the classical and the "kinetic" expression. Their results demonstrate better agreement when

using the "kinetic" theory than when the classical expression is used. The nucleation rate I derived from this theory is:

$$I = \frac{\beta_{11} n_s^2 S}{12} \sqrt{\frac{\theta}{2\pi}} exp[\theta - \frac{4\theta^3}{27(lnS^2)}] \tag{2.23}$$

Where β_{11} is the Brownian coagulation coefficient between two monomers.

2.4.2 Condensation

After the iron particles are formed by homogeneous nucleation and a high concentration of particles are present, and the saturation ratio is low but greater than one, condensation takes place on the existing particles. Surface condensation is the deposition of monomers on a stable particle, of size equal to or larger than the critical size. The rate of heterogeneous condensation depends on the exchange of matter and heat between a particle and the continuous phase. Assuming that the size of a monomer is negligible compared to that of the particle, the growth law of a spherical particle in the free molecular regime is given by

$$\frac{dv_i}{dt} = B_i v_i j^{2/3} (S - 1) \tag{2.24}$$

with

$$B_1 = (36\pi)^{1/3} n_s v_1^{2/3} (k_B T / 2\pi m_1)^{1/3} \tag{2.25}$$

v_j is the particle volume, v_1 and m_1 are the the volume and the mass of one monomer.

In the production of iron particles, the size of the end product from this model is between 10 and 100 nm in diameter. This range of sizes falls between the free molecular range and the transition to the continuum range

2.4.3 Coagulation

The evolution of the concentration (n_j) of stable particles of size j by coagulation due to Brownian motion is described by the Smoluchowski balance equation:

$$\frac{\partial n_j}{\partial t} = \frac{a}{2} \sum_{i=j^*}^{j-1} \beta_{i,j-i} n_i n_{j-i} - a n_j \sum_{i=j^*}^{\infty} \beta_{ij} n_i \tag{2.26}$$

where a is the sticking coefficient, meaning the fraction of interparticle collisions that result is coalescence. The coagulation coefficient $\beta_{i,j}$ between spherical particles contain-

ing, respectively, i and j monomers of one single chemical especies is give in the free molecular regime by [41];

$$\beta_{i,j} = (\frac{3v_1}{4\pi})^{1/6}\sqrt{\frac{6K_BT}{\rho_p}(\frac{1}{i}+\frac{1}{j})}\cdot(i^{1/3}+j^{1/3})^2 \tag{2.27}$$

in which ρ_p is the particle density.

Once the different forms of the internal processes are discussed, the addition of the effect of internal plus the external processes on the particle size distribution will lead to the General Dynamic Equation.

2.5 General dynamic equation of aerosols

In order to obtain a simplified system, only stable populations of aerosol issue of homogeneous nucleation are considered. Having described the influence of transport and aerosol growth mechanisms affecting the particle size, the dynamic equation in a discrete representation is as follows:

$$\frac{\partial n_j}{\partial n} = I\delta_{(j-j^*)} + G_{j-1}n_{j-1} - G_jn_j + \frac{1}{2}\sum_{i=j^*}^{j}\beta_{j,j-i}n_jn_{j-i} - n_j\sum_{i=j^*}^{\infty}\beta_{i,j}n_i \tag{2.28}$$

The $\delta_{(j-j^*)}$ has a value of 1 for $j = j^*$ and 0 for any other j.

2.5.1 Solution of the general dynamic equation of aerosols

The non-linear, partial integro-differential equation described before must to be solved numerically because of its complexity. This equation is normally coupled with the environment; momentum, heat and equations for the chemical species. At this point numerical solutions are useful. Even though numerical solutions can deal with complex non-linear equations, they have one great disadvantage over analytical solutions, the lack of generality. Besides, numerical solutions normally take a lot of computational time and effort, and Parametric analysis is not as straight forward as for analytical solutions.

A particle of aerosol is formed by a entire number of monomers, atoms or basic molecules. Several representations are used in mathematic models for approximating a size distribution. Considering the classification of models made by Seigneur(1986)[42], next models are found:

a) Continuous representations The continuous model solves the continuous general dynamic equation for a finite number of particle sizes and the values between them are interpolated by either a straight line or a cubic spline [11]. One of the disadvantages of this method is that the evolution of the particel size-distribution might be inaccurately represented, especially in the size range where the distribution changes suddenly with the particle size or where discrete size effects are important.

b) Discrete representations This kind of model solves the discrete form of the general dynamic equation. It gives the most accurate result because the rate equation for the population of each particle size is exactly described by one equation without using any mathematical approximation for the particle size distribution. However, because one partial differential equation is needed for every single particle size, the computation becomes intractable when it is extended to particles formed of a few thousands of monomers. This approach is restricted to cases with very narrow size distributions and for very short periods of time.

c) Discrete-continuous representations It was developed by Gelbard et all. [14] in order to overcome the limitations of the purely discrete or continuous methods in solving the general dynamic equation over a broad particle size spectrum. This method covers the entire size range by dividing the particle size distribution into two regimes: for particles smaller than a specific size, the discrete representation is used, whereas for large particles, a continuous representation of the general dynamic equation is used.

d) Sectional representations Discrete-continuous method failed in some cases because it generated negative values for the particle concentration due to the interpolation of the size distribution. The introduction of sectional methods solves this problem. In this so-called sectional model, the size domain is divided into sections, only one integral quantity (e.g. number, surface area, or volume) is considered in each section. This method has the advantage that the integral quantity is conserved within the computational domain and coagulation between all particle sizes is properly accounted.

e) Parametric representations A parametric representation calls upon hypotheses on the form of the distribution of sizes of particles. The population is thus characterized by a small number of parameters. These formulations need the solution of a small number of differential equations and often are applied to the studies of simulation implying two spatial dimensions. The moment method which results in only four partial differential equations to describe the evolution of the particle size distribution, is sufficiently efficient and economical to be extended to more dimensions.

Discrete, continuous and sectional models could solve the evolution of the detailed particle distribution; however their applications are limited to one-dimensional cases, making them unattractive when particle transport is to be considered. In order to extend the solution of the general dynamics equation to a two-dimensional case, a simpler approach is needed. The method of moments which is part of the parametric representations model, is a good choice to surmount this problem.

The method of moments

The method of moments is based on the description of the aerosol evolution by moments of the particle size distribution function (e.g., total number, total surface area, total mass, etc.). The method has been repeatedly explored for aerosol dynamics. The underlying idea of the approach is that the properties one considers in most practical applications are determined by average measures [43], [30]; the history of individual particles can be ignored, and what is lot in accuracy and resolution is compensated for by a significant increase in computational speed and a dramatic reduction in computer memory requirements.

Moments of a distribution are global parameters which describe important properties of the distribution. It means, a property ψ with exponent k is used for weighting concentrations. This property ψ can be i.e. the number of monomers contained in a particle, the volume, the diameter, the concentration or the age of a particle. In this way, only considering stables particles, the order k moment is represented for a discrete distribution and for a continue distribution:

$$M_k = \sum_{j=j^*}^{\infty} \psi^k n_j \tag{2.29}$$

$$M_k = \int_{j=j^*}^{\infty} \psi^k n_j d_j \tag{2.30}$$

For the present work, the ponderation by the number of monomers contained by the particles is used, being given his conservation by the different mechanisms growth. The equation for moments becomes:

$$M_k = \sum_{j=j^*}^{\infty} j^k n_j \tag{2.31}$$

In this way, next table presents the different physical properties of an aerosol can be obtained since these distribution moments weighting for a number of monomers contained by particles [1].

Table 2.2: MAIN PHYSICAL PROPERTIES IN FUNCTION OF MOMENTS

Independent Property	*Function of moments*
Total concentration, N	M_0
Mean numeric diameter	$d_1 \frac{M_{1/3}}{M_0}$
Mean mass diameter	$d_1 \frac{M_{4/3}}{M_1}$
Standard deviation over numerical diameter, σ_d^2	$d_1^2(\frac{M_{2/3}}{M_0} - \frac{M_{1/3}^2}{M_0^2})$
mean surface, $\overline{s}$	$s_1 \frac{M_{2/3}}{M_0}$
mean volume, $\overline{v}_p$	$v_1 \frac{M_1}{M_0}$
Standard deviation over volume, σ_v^2	$v_1^2(\frac{M_2}{M_0} - \frac{M_1^2}{M_0^2})$
mean geometric volume, v_g	$\frac{M_1^2}{M_0^{3/2} M_2^{1/2}}$
Geometric standard deviation over volume,σ_g	$ln^2\sigma_g = \frac{1}{9}\frac{M^0 M_2}{M_1^2}$

Fractional moments presented in table 2.2 don't have a physical explanation. They are reduced moments of fractional order which are interpolated from the integer and known fractional moments. The number concentration, surface, and mass particles in a given volume are obtained, respectively, from the moments of order 0, 2/3, and 1. In the present model, the moments of order 0, 1, and 2 are solved. Therefore, the fractional moments that appear in the conservation equations are estimated assuming that the size distribution is lognormal. More information is found in [18].

The lognormal distribution function The size distribution function of a collection of particles can be defined in terms of any parameter that characterizes any particle (e.g. particle diameter, particle mass, particle volume,etc). Also, the particle size distribution can be represented in a discrete or in a continuous form. The function of the concentration of particles of size j is given by:

$$n_j = \frac{1}{3\sqrt{2}\pi ln\sigma_g} exp[-\frac{ln^2(\frac{v_j}{v_g})}{18ln^2\sigma_g}]\frac{1}{v_j} \tag{2.32}$$

A closed system can be obtained for describing the evolution of distribution moments in function of themselves by different growth mechanisms. It will be described in the next chapter.

2.6 Description of the process to be modelled

The present work accounts for modelling the synthesis of nanoparticles produced by gas condensation. The entire process consist the evaporation of a metal into inert gas in a hot plasma section. This part is not accounted for the present simulation, however, the information about velocity, temperature, and mass fraction profiles are considered since [1]. In a following step, for which this model applies, the metal vapor and inert gas are transported into a second vessel in which condensation takes place and the particles are produced.

The mathematical model is applied to an induction plasma reactor for the preparation of ultrafine iron powders. The reactor described by Girshick et al. (1993)[6] as shown in figure 2.3 was found by [1] like one to satisfy these needs. Iron powders are injected in the induction zone of a plasma reactor, where they evaporate and form a metal vapor cloud. The induction tube is 0.38 m in length and 0.022 m in radius, and ends in a wider condensation tube. Argon gas at room temperature is injected uniformly through the porous wall of the last section, which is 1 m long and has a radius of 0.032 m. This causes a rapid temperature decrease of the jet and the condensation of the vapor in a fine aerosol.

The present study assumes that the temperature of the gas inside the plasma chamber is high enough so that particles are only formed inside the particle generator. Inside this reactor, due to the temperature decrease, the saturation ratio of the metal vapor increases up to the point where homogeneous nucleation starts to form particles; the saturation ratio is further decreased by condensation of metal atoms on the surface of the existing particles. If concentration of particles is high enough, collisions between them become important, thus affecting the growth of particles by coagulation.

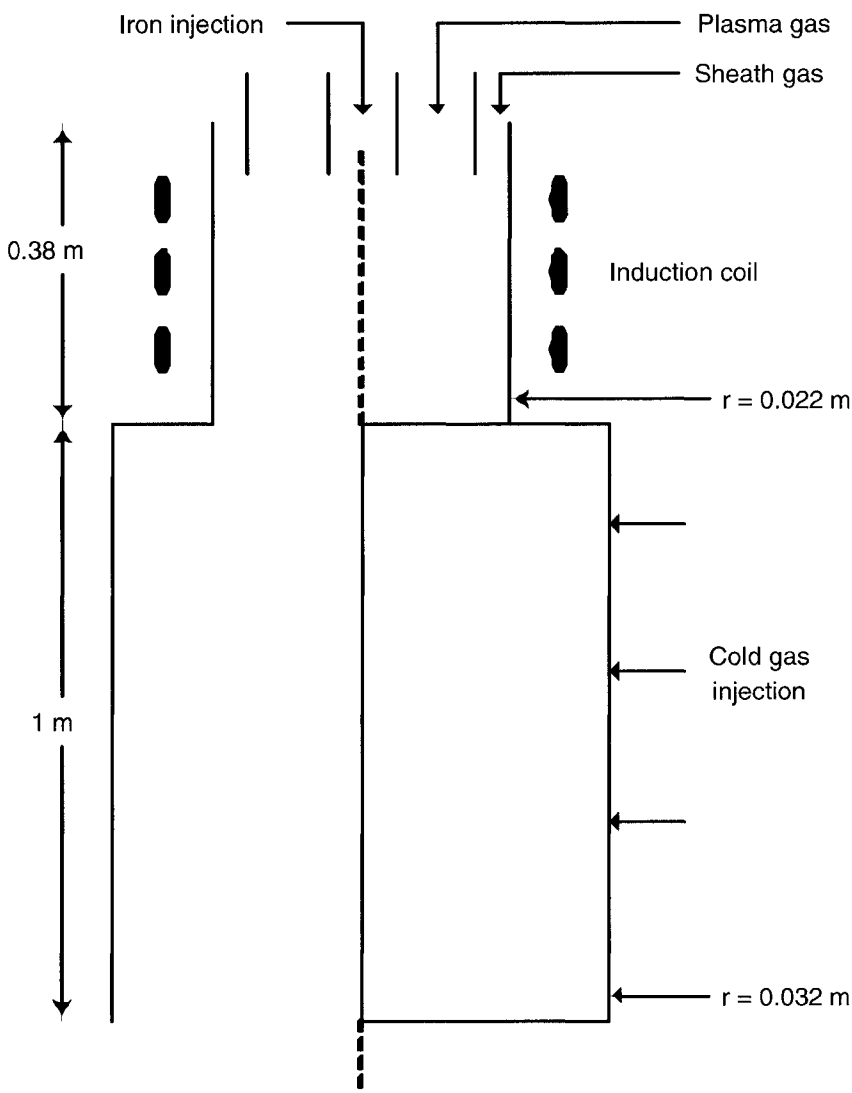

Figure 2.3: Ultrafine iron particle reactor

Chapter 3

MATHEMATICAL RELATIONS AND CFD MODELING

Modeling process requires the use of data from experiments or texts to find simplifying assumptions and translate the physical phenomenons into equations. These equations were presented in chapter 2, next step of modeling process is to solve them.

3.1 Momentum and energy equation

The assumptions and approximations used for this first part of the model are presented bellow followed by the corresponding set of equations to be solved (fluid flow and energy field).

3.1.1 Assumptions for fluid flow

To simplify the solution of the equations of the model it is assumed that the system is symmetric with respect to the center line of the reactor. The density of the gas is calculated using the ideal gas law due to the low pressure and relative high temperature process. Other assumptions are also presented in table 3.1 :

3.1.2 Equations for momentum and energy equation

The general conservation equation proposed by Patankar [25] is as follows:

$$\frac{\partial}{\partial t}(\rho\phi) + \vec{\nabla} \cdot (\rho \vec{u} \phi) = \vec{\nabla} \cdot (\Gamma_p \vec{\nabla} \phi) + S_c + S_p \phi \tag{3.1}$$

The source term S is linearized and dissociated in two parts: S_c is the constant term and $S_p = \frac{\partial S}{\partial \phi}$ is the slope of the variable ϕ. Using this technique with an artificial negative

Table 3.1: FLUID FLOW AND TEMPERATURE FIELD ASSUMPTIONS

Assumptions - Fluid Flow and Temperature Fields
✓ Steady State
✓ Axi-symmetric flow and permanent regime
✓ Turbulence modeled by the K-epsilon model
✓ Particles do not affect the fluid field or the turbulent quantities
✓ The latent heat of phase transition is neglected
✓ Radiative losses are neglected
✓ The physical properties such as viscosity and thermal conductivity are those of the gas-dilute system

slope is a numerical "trick" which allows to get stabilization for the equations solution process. All involved terms in this equation are presented in table 3.1.

3.2 Conservation of species and moment equations

This section describes the formulation of the particle population balance, considering the different mechanisms of transport and growth. These contributions are translated in terms of moments of the distribution, therefore conservations for the moments of the particle's size distribution are obtained.

3.2.1 General dynamic equation over an element of volume

The formulation of a balance in an volume element allows to consider the particle diffusion and aerosol diffusion, both at the same time in the overall domain. In this situation, it is possible to apply the source terms to the right equation. Applying the conservation of particles in a volume element considering thermophoresis, the general transport equation for particles transport is:

$$\frac{\partial n_j}{\partial t} + \vec{\nabla} \cdot (\vec{u} n_j) = -\vec{\nabla} \cdot (\vec{u}_{th} n_j) + \vec{\nabla} \cdot (D_j \vec{\nabla} n_j) \tag{3.2}$$

If the last equation is added to the general dynamic equation for a discrete distribution, the general conservation equation of particles over an element of volume becomes:

$$\frac{\partial n_j}{\partial t} + \vec{\nabla} \cdot (\vec{u} n_j) = -\vec{\nabla} \cdot (\vec{u}_{th} n_j) + \vec{\nabla} \cdot (D_j \vec{\nabla} n_j) + G_{j-1} n_{j-1} - G_j n_j + \frac{1}{2} \sum_{i=j^*}^{j} \beta_{j-i,i} n_i d_i - n_j \sum_{i=j^*}^{\infty} \beta_{j,i} n_i d_i \tag{3.3}$$

3.2.2 Assumptions and description in terms of moments

The moments of the size distribution are defined since the discrete representation and normalized by the density and by a reference concentration of monomers n_0 at the enter of the reactor:

$$M_k = \frac{1}{\rho n_0} \sum_{j=j^*}^{\infty} j^k n_j \tag{3.4}$$

This formulation ensures the conservation of moments in the general equation used if the general conservation of mass is respected. The conservation equation in terms of moments can be obtained by sum over the distribution:

$$\frac{dM_k}{dt} = \frac{d}{dt}\left(\frac{1}{\rho n_0} \sum_{j=j^*}^{\infty} j^k n_j\right) \tag{3.5}$$

With the goal of translating the equations describing the growth of nanoparticles in terms of the moments and to get a closed system, the particle flow and their generation rate must to be expressed according to a polynomial function of size.

There are several assumptions that limit the application of the current model. The first one is the dilute system assumptions which does not allow metal vapor concentrations greater than 10^{-3} kg/kg. Other assumptions such as the size of the particles smaller that the mean free path of the gas limit the use of the model to nanoparticles smaller than 150 nm. Despite these limitations, these assumptions help to greatly simplify the model, since the coagulation and condensation rate are also in the free molecular regime. Furthermore, the assumptions are greatly justified under the conditions used to generate nanoparticles in thermal plasmas [1].

The most important simplification of the model is the assumption of a lognormal particle size distribution function representing the particles at any place in the reactor. Using this hypothesis, it is possible to calculate the different moments of the particle size distribution in a closed form using only the first three moments of the distribution. The main outcome if this approximation is the simplification of the equations to be solved,

from a partial integro-differential (the GDE) equation to a set of three partial differential equations. It is also implicit in this assumption of lognormal distribution that the particles are all spherical and do not form aggregates. In other terms, the present model is limited to the phase of growth of nanopraticles which forms the spherical particles found in fractal aggregates.

Next table presents important assumptions to simplify the solution of equations describing the evolution of the particle size distribution along the reactor.

Table 3.2: METAL VAPOR CONCENTRATION AND MOMENT EQUATION EQUATIONS ASSUMPTIONS

Assumptions - Metal vapor concentration and moment equations
✓ Particles are smaller that the mean free-path of the gas: free-molecular regime
✓ Coagulation of particles takes place in the free-molecular regime
✓ Condensation of metal vapor on existing particles is governed by molecular bombardment (free-molecular regime)
✓ The kinetic nucleation rate developped by Girshick [38] is used
✓ The particle size distribution can be approximated by a lognormal distribution
✓ Particles are spherical and structureless, no agglomerates are formed.
✓ The Kelvin effect is neglected
✓ Calculation of the volume of particles are based on the bulk density of iron
✓ Capillarity approximation
✓ There are no particles entering the reactor
✓ Particles follow the fluid flow and are only deviated by Brownian diffusion

The contribution of the different mechanisms (nucleation, condensation, coagulation, thermophoresis) are transformed next in terms of moments of the distribution.

Nucleation

The homogeneous nucleation produces particles of size j^* [38]. In this way the equation that describes the evolution of the concentration of particles of size j is:

$$\frac{dn_j}{dt} = I\delta_{j-j^*} \tag{3.6}$$

The δ_{j-j^*} expression has a value of 1 for the critical size j^*. The integral over the size distribution gives the expression for the distribution moments:

$$\frac{\rho M_k}{dt}(nucl) = \frac{I}{n_0}(j^k) \tag{3.7}$$

Condensation

The expression for the condensation in an homogeneous medium, results from adding the contribution of the growth law by condensation in the free molecular regime overall the distribution:

$$\frac{\rho M_k}{dt}(cond) = \rho k B_1 (S-1) M_{k-1/3} \tag{3.8}$$

Coagulation

In the goal of translate the contribution of the coagulation term in function of distribution moments, Frenklanch (1987) [44] proposes three methods for the free molecular regime. The first method estimates the mean coagulation coefficient with the overall distribution instead while the second uses a summation over all collision. Bilodeau[1] proposes a combined method yielding a mean coagulation coefficient since the set of collisions.

Adding the coagulation term over the whole distribution:

$$\frac{\rho M_k}{dt} = \frac{1}{2n_0}\sum_{j=j^*}^{\infty}\sum_{i=j^*}^{j} j^k \beta_{i,j-i} n_i n_{j-i} - \frac{1}{n_0}\sum_{j=j^*}^{\infty}\sum_{i=j^*}^{\infty} j^k \beta_{i,j} n_j n_i \tag{3.9}$$

Changing variable m=j-i in the first sum and doing $n_j = 0$ for j less to j^*, we find:

$$\frac{\rho M_k}{dt} = \frac{1}{2n_0}\sum_{j=j^*}^{\infty}\sum_{i=j^*}^{\infty}[(j+i)^k - 2j^k]\beta_{i,j} n_j n_i \tag{3.10}$$

$$\frac{\rho M_k}{dt} = \frac{C}{2n_0}\sum_{j=j^*}^{\infty}\sum_{i=j^*}^{\infty}[(j+i)^k - 2j^k]\sqrt{\frac{1}{i}+\frac{1}{j}}(i^{1/3}+j^{1/3})^2 n_i n_j \tag{3.11}$$

with:

$$C = (\frac{3v_1}{4\pi})^{1/6}\sqrt{\frac{6K_B T}{\rho_p}} \tag{3.12}$$

The coagulation equation can be written as:

$$\frac{\rho M_k}{dt} = \frac{C}{2n_0}\sum_{j=j^*}^{\infty}\sum_{i=j^*}^{\infty}[(j+i)^k - 2j^k] + \frac{(1+j)^{1/2}}{\sqrt{ij}}(i^{1/3}+j^{1/3})^2 n_i n_j \tag{3.13}$$

The functions $f_{x,y}^r$ are defined as follows:

$$f_{x,y}^{r} = \sum_{j=j^*}^{\infty} \sum_{i=j^*}^{\infty} (i+j)^r \frac{(i^{1/3}+j^{1/3})^2}{\sqrt{ij}} i^x j^y n_i n_j \tag{3.14}$$

Analog functions in later sums are used to approximate the evolution of the distribution of moments by brownian coagulation in the free molecular regime:

$$\frac{d(\rho M_0)}{dt}(coag) = -\frac{\rho^2 n_0}{2} \Phi_{0,0} M_0^2 \tag{3.15}$$

$$\frac{d(\rho M_1)}{dt}(coag) = 0 \tag{3.16}$$

$$\frac{d(\rho M_2)}{dt}(coag) = \rho^2 n_0 \Phi_{0,0} M_1^2 \tag{3.17}$$

$\Phi_{0,0}$ is the mean collision coefficient averaged over the collisions ($m^{-3}s^{-1}$) and is estimated by logarithmic interpolation between the functions $f_{0,0}^0$, $f_{0,0}^1$,$f_{0,0}^2$

$$\Phi_{0,0} = C\binom{0}{f_{0,0}}^{3/8} + \binom{1}{f_{0,0}}^{3/4} + \binom{2}{f_{0,0}}^{-1/8} \tag{3.18}$$

It is necessary to bring the functions $f_{0,0}^r$ into the normalized distribution of moment terms:

$$f_{0,0}^0 = 2(\mu_{-1/2}\mu_{1/6} + \mu_{-1/6}^2) \tag{3.19}$$

$$f_{0,0}^1 = 2(\mu_{-1/2}\mu_{7/6} + 2\mu_{-1/6}\mu_{5/6} + \mu_{1/6}\mu_{1/2}) \tag{3.20}$$

$$f_{0,0}^2 = 2(\mu_{-1/2}\mu_{13/6} + 2\mu_{-1/6}\mu_{11/6} + \mu_{1/6}\mu_{3/2} + 2\mu_{1/2}\mu_{7/6} + 2\mu_{5/6}^2) \tag{3.21}$$

Where μ_k is the dimensionless moment of order k defined as M_k/M_0. In this way we have a system of moment functions of the distribution size of particles. The fractional moments required for $\Phi_{0,0}$ are interpolated between the known integer moments.

Convection and thermophoresis

The advection of particles is produced by the gas flow and the thermophoresis deviation. According to [33], the thermophoretical velocity is independent of the particle size in the free molecular regime. The moments of the distribution are moved by this velocity, and by summation over the distribution, we get:

$$\frac{\partial(\rho M_k)}{dt} + \vec{\nabla} \cdot (\rho(\vec{u} + \vec{u}_{th}) M_k) = 0 \tag{3.22}$$

Diffusion

The diffusion coefficient depends on the particle size. Therefore, a global coefficient cannot be applied over the distribution of moments. Nevertheless, because of the importance of this mechanism, a mean diffusion coefficient is defined and calculated from the mean masse diameter of the distribution. The given expression by [33] is used in this work. The contribution of the diffusion term over the evolution of moments is represented by:

$$\frac{\partial(\rho M_k)}{dt} = \overrightarrow{\nabla} \cdot (\rho \overline{D} \overrightarrow{\nabla} M_k) \tag{3.23}$$

$$\overline{D} = \frac{k_B T}{3\pi\mu\overline{d}}(1 + \frac{3.314\lambda}{\overline{d}}) \tag{3.24}$$

$$\overline{d} = \frac{M_{4/3}}{M_1} d_1 \tag{3.25}$$

General equation of moments

The sum of the last overall contributions yields the General Conservation Equation of Moments:

$$\frac{\partial(\rho M_k)}{dt} + \overrightarrow{\nabla} \cdot (\rho \overrightarrow{u}_{th} M_k) = - \overrightarrow{\nabla} \cdot (\rho \overrightarrow{u}_{th} M_k) + \overrightarrow{\nabla} \cdot (\rho \overline{D} \overrightarrow{\nabla} M_k) + \frac{I}{n_0}(j^*)^k + kB_1\rho(S-1)M_{k-1/3} + \frac{\rho^2 n_0}{4}[k^2 + k - 2]\Phi_{0,0}M_{k/2}^2 \tag{3.26}$$

By mass balance over the aerosol and the vapor, the conservation of the monomer in vapor phase is as follows.

$$\frac{\partial(\rho\omega_1)}{dt} + \overrightarrow{\nabla} \cdot (\rho \overrightarrow{u}_{th} \omega_1) = \overrightarrow{\nabla} \cdot (\rho D_1 \overrightarrow{\nabla} \omega_1) - Ij^* m_1 - B_1 \rho n_0 m_1 (S-1) M_{k-1/3} \tag{3.27}$$

3.2.3 Constitutional equations

Moment of order 0

$\Phi \quad = M_0 (m^3/\mathrm{kg})$

$\Gamma \quad = \rho\overline{D}$

$S_c \quad = -\overrightarrow{\nabla}(\rho \overrightarrow{u}_{th} M_0) + \frac{I}{n_0} + \frac{\rho^2 n_0}{2}\Phi_{0,0}M_0^2$

$S_p = -\rho^2 n_0 \Phi_{0,0} M_0$

Moment of order 1

$\Phi = M_1 (m^3/\text{kg})$

$\Gamma = \rho \overline{D}$

$S_c = -\vec{\nabla}(\rho \vec{u}_{th} M_1) + \frac{I}{n_0} j^* + B_1 \rho (S-1) M_{2/3}$

$S_p = 0$

Moment of order 2

$\Phi = M_1 (m^3/kg)$

$\Gamma = \rho \overline{D}$

$S_c = -\vec{\nabla}(\rho \vec{u}_{th} M_2) + \frac{I}{n_0} (j^*)^2 + \rho^2 n_0 \Phi_{0,0} M_1^2 + 2 B_1 \rho (S-1) M_{5/3}$

$S_p = 0$

3.3 CFD modeling

The particle growth process was simulated using the *Computational Fluid Dynamics Code* (CFD) FLUENT© version 6.0. In this research, selected CFD results issued to FLUENT© are compared with those of Bilodeau[1]. Good correlation between bibliography and CFD results is used to *validate* the present CFD model. Model validation increases confidence that all of the CFD results accurately depict real life conditions.

The current CFD model of the nanoparticle growth reactor contains over 9600 cell volumes in an structured mesh format.

3.3.1 Overview of a CFD solution

The solution of a *Computational Fluid Dynamics* problem consists of subdividing the geometry into small control volumes. Three basic principles of physics are applied to the fluid flow in each volume.

1 Mass is conserved

2 Energy is conserved

3 Newton's Law $F = m \cdot a$

These three principles allow governing equations to be derived. The governing equations are nonlinear differential of integral equations that completely describe the flow in each control volume. No direct methods exist for solving these systems of equations. Therefore, the governing equations are linearized and solved numerically.

The two key factors to a successful solution are:

- Good initial guesses to be used by the linear equation solver for model parameters such as flow velocity, pressure and turbulence.
- A well discretized domain.

3.3.2 Building the flow geometry

The first step in the simulation of the nanoparticle growth reactor was to identify the geometric constraints of the problem. In this case, the geometry was that of the reactor described by [6].

This geometry was created using GAMBIT©. GAMBIT© is essentially a simple CAD program integrated into a very advanced meshing program. The tools in GAMBIT© were sufficient for modeling the nanoparticle growth reactor.

The nanoparticle growth reactor was simplified somewhat due to its one line of symmetry. Symmetry reduces the total number of cells, or control volumes, needed to numerically represent the apparatus. Special symmetry boundary conditions in FLUENT© allow this one-half representation to accurately depict the whole.

Creating the computational mesh The nanoparticle growth reactor geometry was meshed using a rectangle control volume shapes.

Mesh quality The quality of the mesh is key to obtaining a converged, accurate solution. A high quality mesh has very uniform cells. In general, all cell edges should be close to the same length.

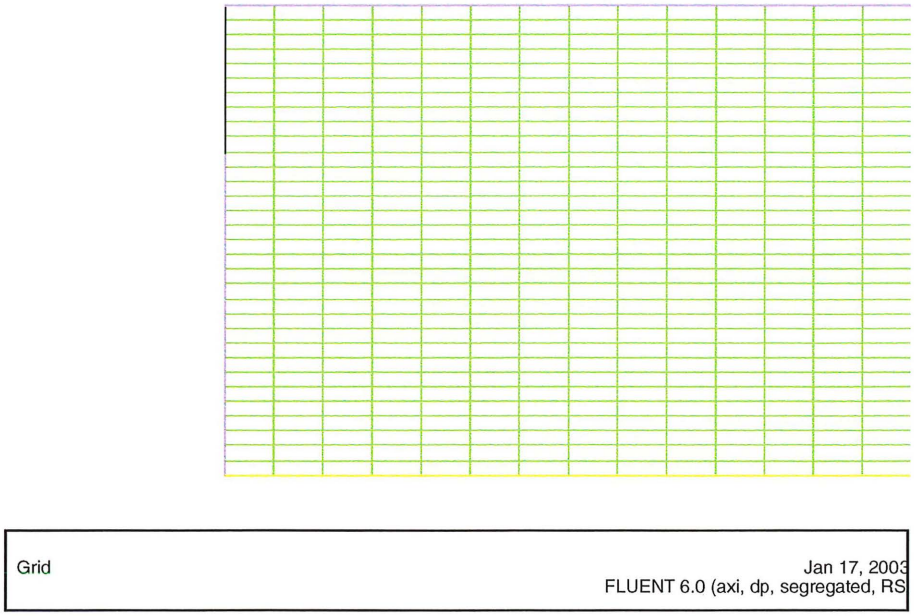

Figure 3.1: Initial grid

There are standard measurements to determine the quality/uniformity of a mesh. These measurements, often called metrics, are covered in detail in the GAMBIT© users guide section 3.4 *Using the global control tool pad* [45].

Two important mesh metrics are aspect ratio, and skew. The aspect ratio is the ratio between the length and height of the cells. In effect, the aspect ratio measures rectangularity for cells. Aspect ratios of up to 1:5 are tolerable for many models.

Skewness can be defined as the difference between the cell's shape and the shape of an equilateral cell of equivalent volume. Highly skewed cells can decrease accuracy and destabilize the solution. For example, optimal quadrilateral meshes will have vertex angles close to 90 degrees, while triangular meshes should preferably have angle of close to 60 degrees and have all angles less than 90 degrees [46].

Boundary conditions Boundary conditions are used to fix flow variables at the limits of a computational grid. Boundary condition availability varies with solver choice. The FLUENT© 6.0 solver includes a wide choice of boundary conditions. Examples of boundary conditions include velocity inlet, wall and symmetry. GAMBIT© applies the boundary conditions to faces. FLUENT© reads these boundary conditions and uses them when solving the systems of linear equations.

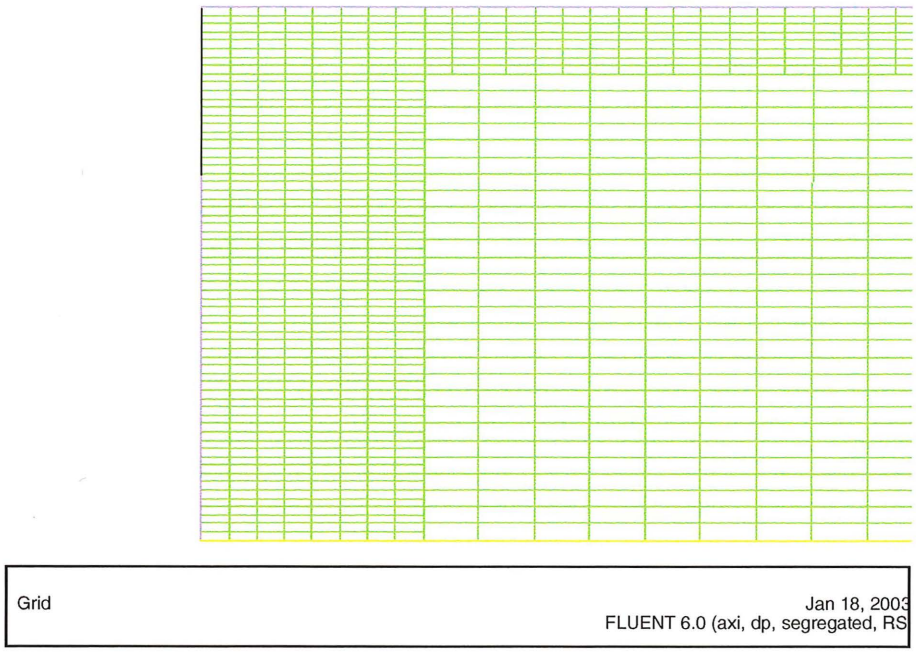

Figure 3.2: Finer grid

When the FLUENT© 6.0 solver is selected in Gambit, all unspecified surfaces will default to the wall boundary condition. Therefore it is not necessary to apply boundary conditions to every surface of the model. The following boundary conditions were used. Later the NAME can be used to aid in the graphical display of model results.

Table 3.3: BOUNDARY CONDITIONS APPLIED TO THE MODEL GEOMETRY

Boundary Condition	*Name*	*Representative of*
Velocity inlet	entree	Gas inlet to the reactor
Wall	paroi1	wall of the reactor
Velocity inlet	paroi2	quenching enter
Velocity inlet	paroi3	quenching enter
Velocity inlet	paroi4	quenching enter
Symmetry	axe	symmetry axis
Pressure Outlet	sortie	outlet

In some cases, there were boundary conditions that could be used as alternatives to those chosen. The best boundary conditions for the model were selected based on their strengths highlighted below.

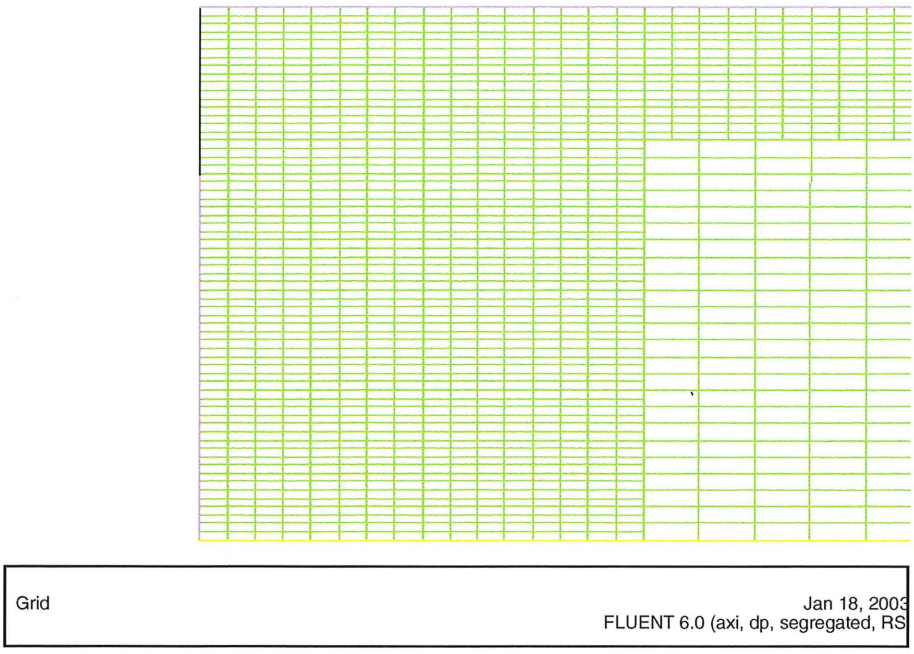

Figure 3.3: Finest grid

- Velocity Inlet. The velocity inlet boundary condition allows the user to specify the fluid velocity and direction using a Cartesian coordinate system. The mass flow is calculated from the velocity. This flow condition is not adequate for compressible flows with high Mach numbers. It is adequate for this application where the flow is incompressible.

- Pressure Outlet. The pressure outlet allows the absolute pressure to be set at the cells where the flow leaves the geometry. Model convergence is possible in cases where turbulence causes flow backwards (backflow) through the outlet.

- Wall. The wall boundary condition fixes the flow to zero on the faces it occupies. By default a no-slip boundary condition is enforced in viscous flows.

- Symmetry. This boundary condition describes the treatment of the flow at symmetry planes. It assumes that there is a mirror image of the model geometry on the other side. For this reason the direction of the flow is unaffected.

Zones Zones are applied to model volumes by Gambit. There are two types of zones, fluid and solid. The type of zones dictates available materials from the Fluent materials panel, and the how Fluent will solve for certain quantities in that zone. In our case we use only fluid zone.

3.3.3 FLUENT© model configuration

Fluent reads the model geometry, boundary and zone conditions from a mesh file exported by Gambit. Additional setup information is necessary before the model can be run. The notation format of MAINmenu:SUBmenu is useful for the description of the Fluent model configuration.

FLUENT© Define: Model: Solver Fluent solves governing equations for conservation of mass and momentum. The Fluent solver will also solve scalar equations including energy balances, turbulence and chemical reactions.

Control volumes have been used to divide the computational domain (the physical model dimensions) into a computational grid. The governing equations are integrated across each of the control volumes. These nonlinear coupled partial differential equations describe the behavior of such variables as velocity, pressure and temperature inside each control volume. The equations are discretized so they may be solved numerically.

The discretized equations are linearized. These linear equations approximate the original nonlinear integral governing equations. Repeated iteration of the linearized discrete equations results in a values which closely approximate those of the original nonlinear integral governing equations.

There are several different methods for linearizing the discretized equations. There are also two options for the general approach to solving this system of linear equations. These methods exist because of limited hardware computational capabilities.

a) *Segregate Solution Method.* The segregate solver solves the governing linear equations once a time. The equations are separated or segregated so that less RAM (Random Access Memory) is required. Only one of the equations is loaded into RAM and solved at one time. The goal is to solve a system of linear equations that are interdependent, or coupled. A special pressure correction allows one equation to be solved at a time while still satisfying the continuity equation.

b) *Coupled Solution Method.* The linearized coupled governing equations (continuity, momentum, energy, species, etc.) may be solve all at once. Other equations (turbulence) are solved sequentially as in the segregated solution method. Though this solution method requires more computational resources (RAM) it does not have to use any correction factors for each of the coupled governing equations. This means the coupled solution technique converges faster and is more robust.

For the development of this model, the segregate solution method (a) was used although the equations are coupled. The reason is that particles are of small size and the metal vapor is at low concentration. Thus, the presence of particles does not affect the momentum or the energy equation and it allows to separate the solution into two parts. The first part deals with the solution of the fluid flow and temperature field by solving the continuity, the momentum in the axial and radial direction, and the energy equation. The second part solves scalars including the conservation of species and the moment equations.

FLUENT© Define: Model: Energy This panel enables the use of the energy balance equations. Additional thermodynamic input become available in the Fluent Define: Boundary Conditions.

FLUENT© Define: Model: Viscous Turbulent flows are characterized by fluctuating velocity fields. These fluctuations mix transported quantities such as momentum, energy, and species concentrations, and cause the transported quantities to fluctuate as well. Since these fluctuations can be of small scale and high frequency, they are too computationally expensive to simulate directly. Instead, the instantaneous (exact) governing equations can be time-averaged, ensemble-averaged, or otherwise manipulated to remove the smaller fluctuations. The result is a modified set of equations that are computationally less expensive to solve. The modified equations contain additional unknown variables, and turbulence models are needed to determine these variables in terms of known quantities.

The default viscous mode is the invicid viscous model. The invicid model totally ignores any effects of viscosity on a flow. It is useful for flows where pressures forces dominate viscous forces. One such example is a model of a speeding bullet where inertial forces tend to dominate viscous forces. The invicid model is also a good starting point for a very complex flow that is difficult to converge,.

A better model for our nanoparticle reactor growth simulation is the standard K-epsilon turbulence model. The standard K-epsilon is a semi-empirical model that is popular because it gives good results with moderate calculation expense. Two equations are used to determine the turbulent velocity and length scales.

FLUENT© Define: Materials Argon-Iron vapor is defined as material with the following characteristics:

FLUENT©Define: Operating conditions Pressure was left as atmospheric, 101325 Pa. The gravity option was no enabled.

FLUENT©Define: Boundary conditions

FLUENT© Solve: Initialize Compute from all cells.

FLUENT© Solve: Iterate Steady State

3.3.4 Judging solution convergence

Convergence occurs when the iterative results returned by the model equations become progressively closer. One popular way to judging convergence is by watching the residuals. Residuals are the difference between the most recent value (for example pressure) and the value from the previous iteration. As the iterations come closer to a solution the residuals become smaller.

Residuals reported by the FLUENT© solver Improvements have been made by Fluent to ease residual interpretation. By default residuals are calculated in fluent using the following formula:

$$RW = \sqrt{\sum (\frac{dW}{dt})^2} \tag{3.28}$$

W represents any variable of interest. The residual W is the average of the squares of all the residuals in each cell of the domain. Time is only important for unsteady state problems. This means that ALL residuals for a particular variable W are RMS averaged and are presented on a graph as a single line.

Typically one would want to compare these residuals to something like an inlet flow rate. A comparison would give perspective as to whether the residuals were small in with respect a known value like inlet velocity. Certain problems including natural convection do not have previously known velocity magnitudes. For this reason, Fluent defaults to residuals in a scaled format. This format allows a more uniform perspective on residual sizes. The residuals are scaled with respect to the largest residual value found in the first five iterations.

Fluent calculates the scaled residual using the following relation where W is any variable of interest.

$$\frac{R(W)_{iterationN}}{R(W)_{iteration5}} \tag{3.29}$$

The scaled residuals are expected to fall about $1x10^{-3}$ but a bad initial guess could make $R(W)_{iteration5}$ very large. This would mean the 10^{-3} order of magnitude for the scaled residual is reached before the solution is actually converged. Monitors of integrated flow variables will help validate the residuals.

However it is important to watch not just the residuals but also an integrated variable (pressure, velocity, etc). This makes possible to judge if the results are coming close to a value or if there still seems to be substantial movement. How close is close enough depends on the specific problem.

FLUENT© model convergence The two following figures (3.4,3.5) represent the convergence of the nanoparticle reactor growth.

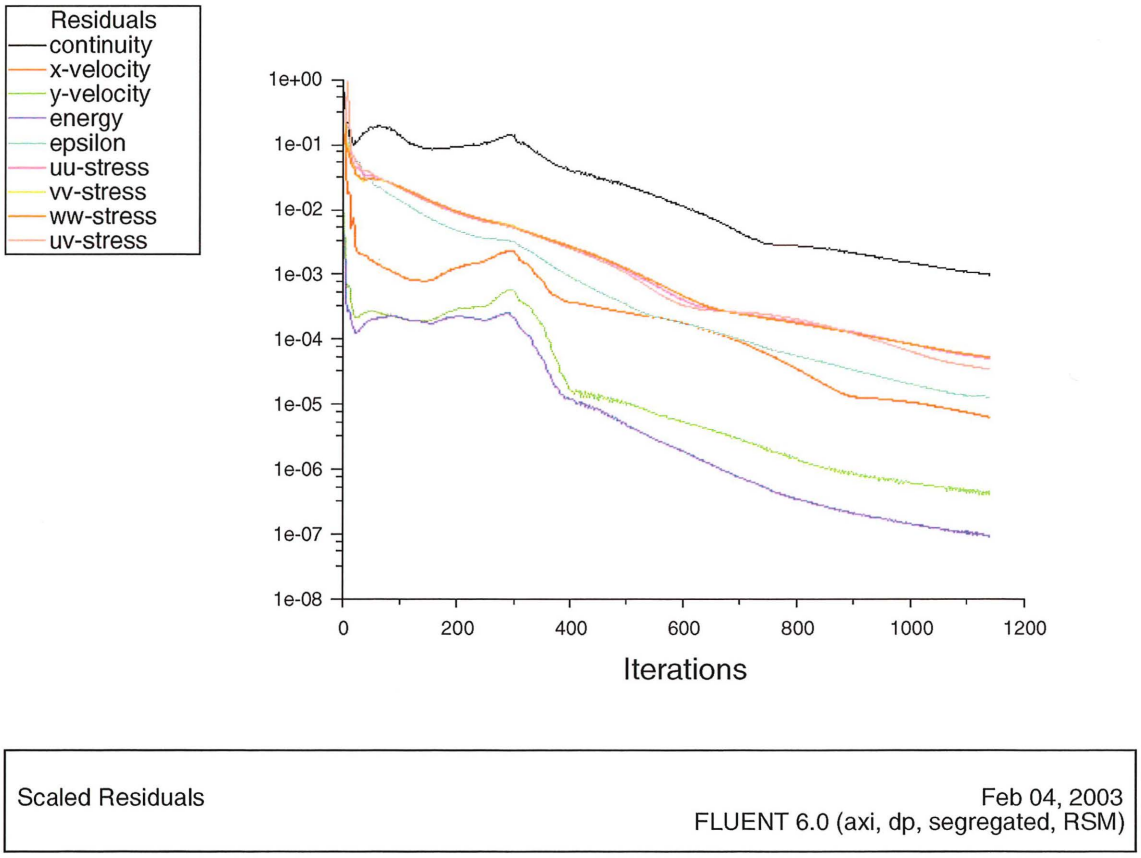

Figure 3.4: Convergence of the fluid dynamics

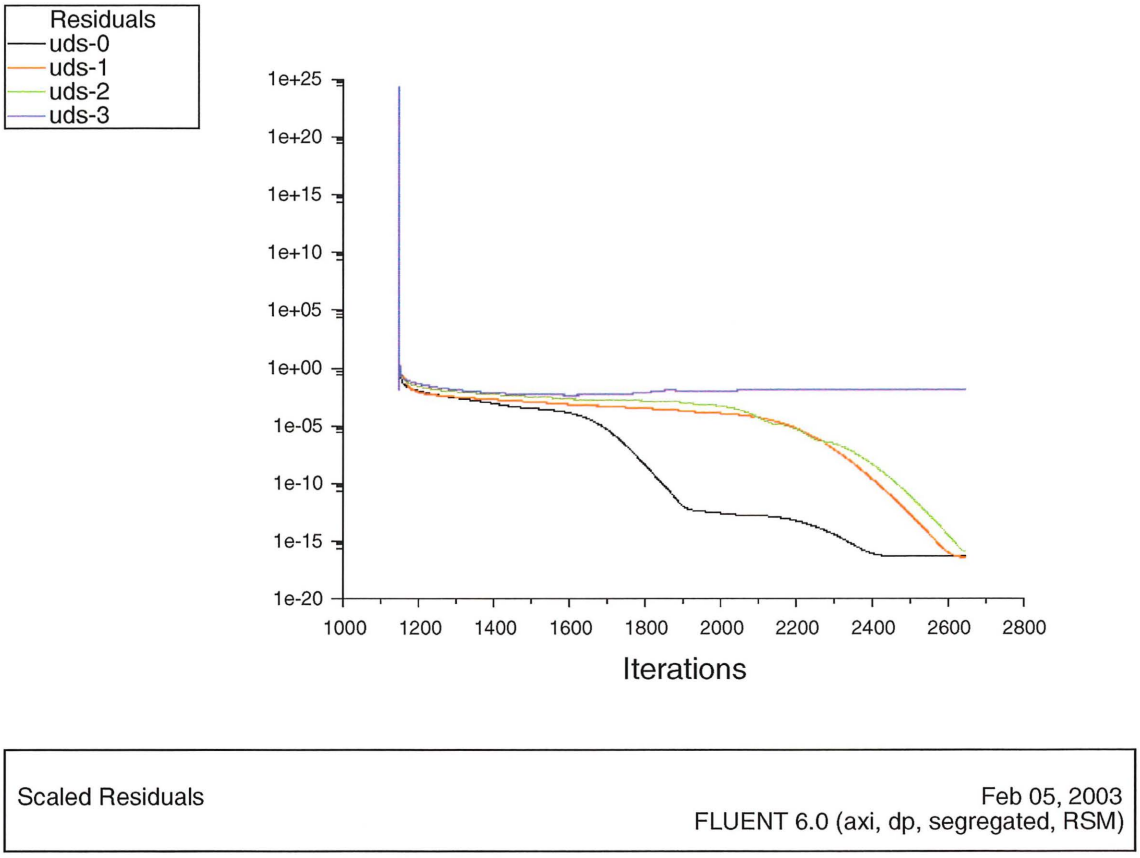

Figure 3.5: Convergence of the scalars

This is a steady state model. This plot suggest good convergence of the steady state temperature model. Based on residual plots, and plots of temperature and scalars, it is safe to say the model has converged.

Chapter 4

RESULTS

The zone of nanoparticle growth for a plasma reactor was simulated by using FLUENT© version 6.0 as CFD. This zone begins at an axial position corresponding to x=0.21 m from the induction zone of the figure 2.3 as describe by Bilodeau (1994)[1]. The system is formed by a metal vapor which is a diluted mix of iron-argon. The operating conditions are presented in the table 4.1 below, as the basis case used for this simulation:

Table 4.1: CONDITIONS OF THE BASIS CASE

Grid Size	Quenching Flow (lpm)	Iron Concentration (kg/kg_{Ar})
Finer	118	$1x10^{-3}$

Upon the basic case, the effect of the metal concentration and quench flow rate variation will be studied as follows in table 4.2.

Table 4.2: PARAMETER VARIATION

Grid Size	Quenching Flow (lpm)	Iron Concentration (kg_{iron}/kg_{Ar})
fine	0	$1x10^{-4}$
finest	236	$1x10^{-5}$
		$1x10^{-6}$

All results, excepting the mass fraction contours of figures 4.4, 4.5, and 4.6, are shown as xy plots. The x axe corresponds to the long of the reactor, that means, 1.0 m. The y axe is the parameter to be analyzed. Results are for four different radial positions of the reactor, as described in table 4.3. Note that the radial value 0.0(line-0mm), corresponds to the axis of the geometry and 0.032(line-32mm) represents the wall of the reactor.

Table 4.3: RADIAL POSITIONS TO BE PLOTTED

Radial value *[m]*	Name
0.0	line-0mm
0.011	line-11mm
0.022	line-22mm
0.032	line-32mm

4.1 Analysis of fluid flow fields

The transport by convection of nanoparticles through the reactor is caused by the fluid flow field, therefore it influences properties of the final product. Main fluid fields concerning the nanoparticle production are temperature and metal vapor concentration. The analysis is presented below .

4.1.1 Temperature field

The temperature field is one of the most important variables in the model since it affects all other equations. The momentum equations are coupled to temperature by viscosity and the continuity equation by density. Species distributions depend on the temperature variation of diffusivity. The particle generation location is determined by the saturation ratio of the metal vapor which is an exponential function of temperature. Finally the size distribution is affected by the local supersaturation and rates of condensation and coagulation are temperature dependent.

Influence of the Quenching Flow Rate on Temperature Field

The injection of cold argon gas through the porous wall causes strong temperature gradients, especially near the wall. Temperature is affected in different way according to the quenching rate injected. Isocontours of the temperature field with the three different quenching rates are shown in figures 4.1, 4.2 and 4.3.

The absence of a quenching rate produces a larger high temperature zone and the reduction of temperature gradients, as shown in figure 4.1. The temperature over the axis

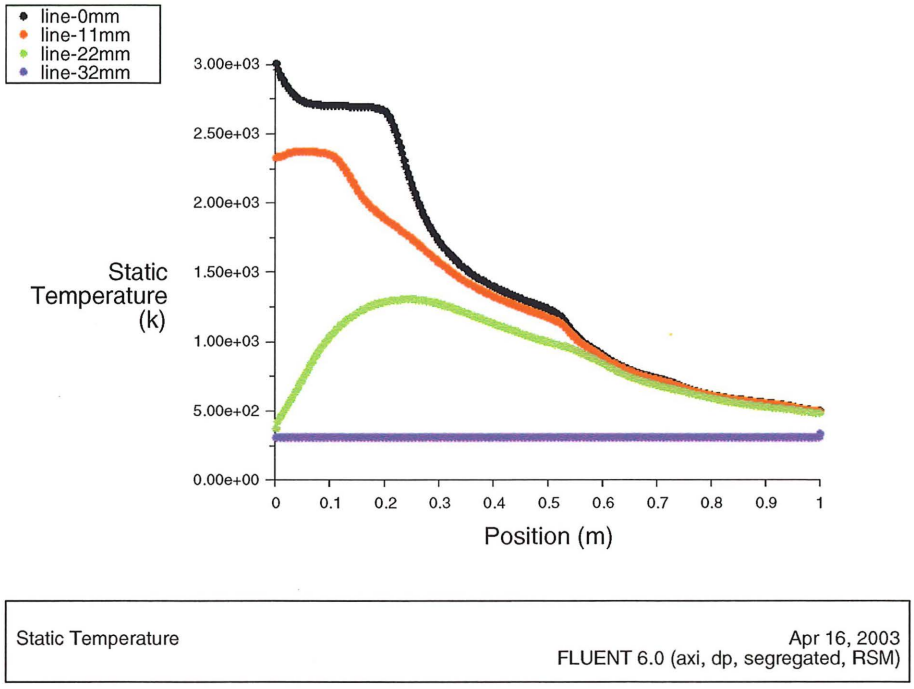

Figure 4.1: Influence of 0 lpm quenching rate on temperature

is controlled by two competitive phenomena: the dilution by a cooler gas decreases the temperature, instead of total flow produces an acceleration in the flow and it increases the temperature over the axis. Figures 4.2 and 4.3 confirm that the increasing of the quenching flow rate produces a decreasing of the large of the high temperature zone and stronger gradients in this zone.

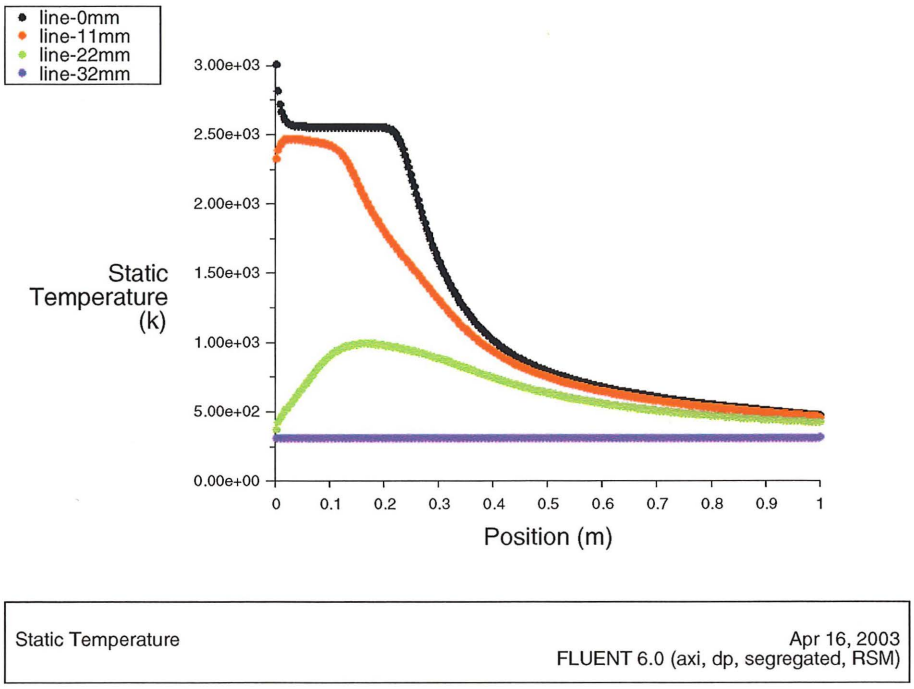

Figure 4.2: Influence of 118 lpm quenching rate on temperature

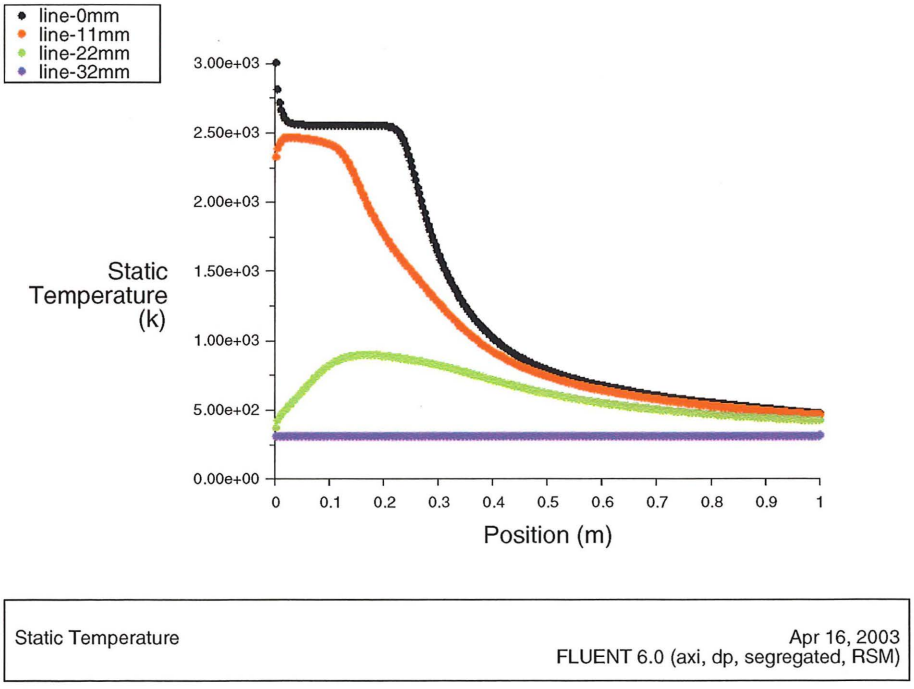

Figure 4.3: Influence of 236 lpm quenching rate on temperature

4.1.2 Metal vapor concentration field

According to the first part of the model of Bilodeau[1], the metal vapor diffuses radially in the induction tube and condenses near the wall due to the lower temperatures encountered there. Immediately, the gas is depleted of metal vapor and enters to the condensation zone. This phenomena of condensation is studied by the present simulation in order to check the nanoparticle formation. Therefore, isocontours of the metal vapor concentration using three different flow rate quenching in the condensation zone are given in following figures.

Influence of the Quenching Flow Rate on Metal Vapor Concentration Field

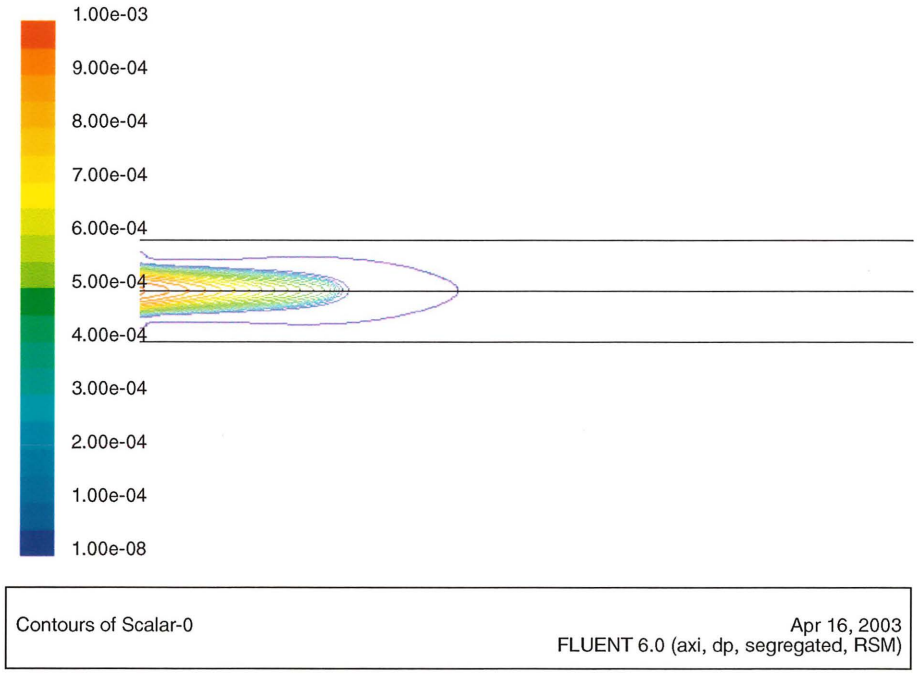

Figure 4.4: Mass fraction without quenching

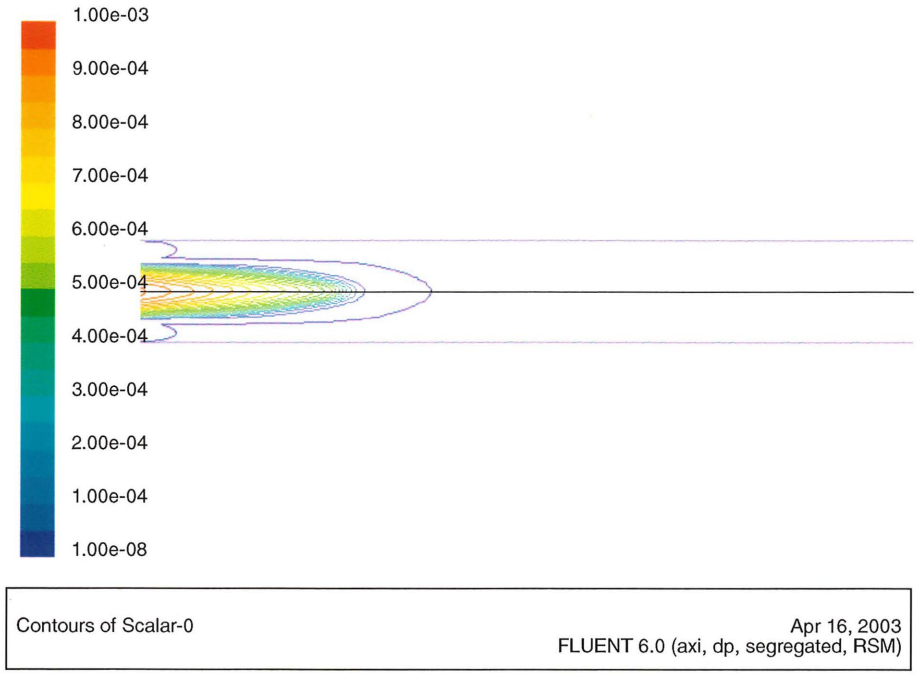

Figure 4.5: Mass fraction with a 118 lpm quenching

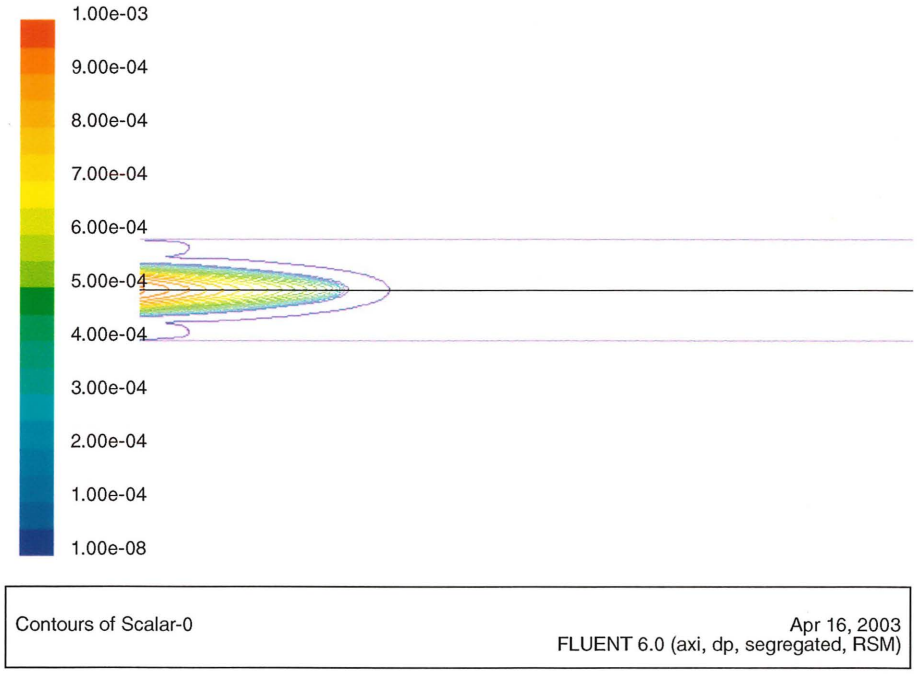

Figure 4.6: Mass fraction with a 236 lpm quenching

Figures 4.4, 4.5 and 4.6 show how the metal vapor concentration is lowered quite fast from $1x10^{-3}$ to $1x10^{-8}$ kg_{Fe}/kg_{Ar}. This is because of the formation of nucleation of particles and because of the condensation of metal vapor on the surface of existing particles. We can also add that the concentration decreases by dilution by the quenching

gas. Near the axis, the slower cooling retards the onset of condensation is noted. However the central cloud is gradually depleted by radial diffusion towards zones where vapor is condensed.

4.2 Analysis of the Nanoparticle Growth

The nanoparticle growth is represented by a log-normal distribution function. Since this, it is possible to describe the particles by three parameters, the particle number density or particle concentration, the particle geometric mean diameter and the geometric standard deviation. The method of moments solves for the first three moments of the particle size distribution. It is possible to give a physical interpretation to the first two moments, but the interpretation of the third one is not straightforward. Therefore, instead of presenting the first three moments of the particle size distribution it is customary to present only the particle number density, geometric mean diameter and geometric standard deviation.

It is known that the quality of the end product depends on the operating parameters; some of the characteristics of the product can intuitively be drawn from changes in the operating conditions. The nanoparticle growth is studied by considering the effect of the quenching flow rate and the metal concentration variation.

4.2.1 Influence of the quenching flow rate on the nanoparticle growth

Increasing the amount of quenching gas should increase the amount of material being condensed. This increase may also affect other parameters such as the nucleation rate, thermophoresis, and coagulation.

The quenching gas flow rate was set from 0 to 236 lpm as the reference case of Bilodeau(1994) [19]. All other parameters were maintained constant.

Particle number concentration

The analysis of the particle number concentration is considered as an important parameter for judging a good reactor performance. The particle number concentration or particle number density (i.e. the number of particles per unit of volume of gas), can be affected by only two of the three processes that modify the particle distribution,

nucleation and coagulation. Nucleation is responsible of the formation of new particles, therefore it causes an increase in the concentration. In another hand, coagulation which is the combination of small particles to form bigger ones, represents the decrease in the particle number concentration.

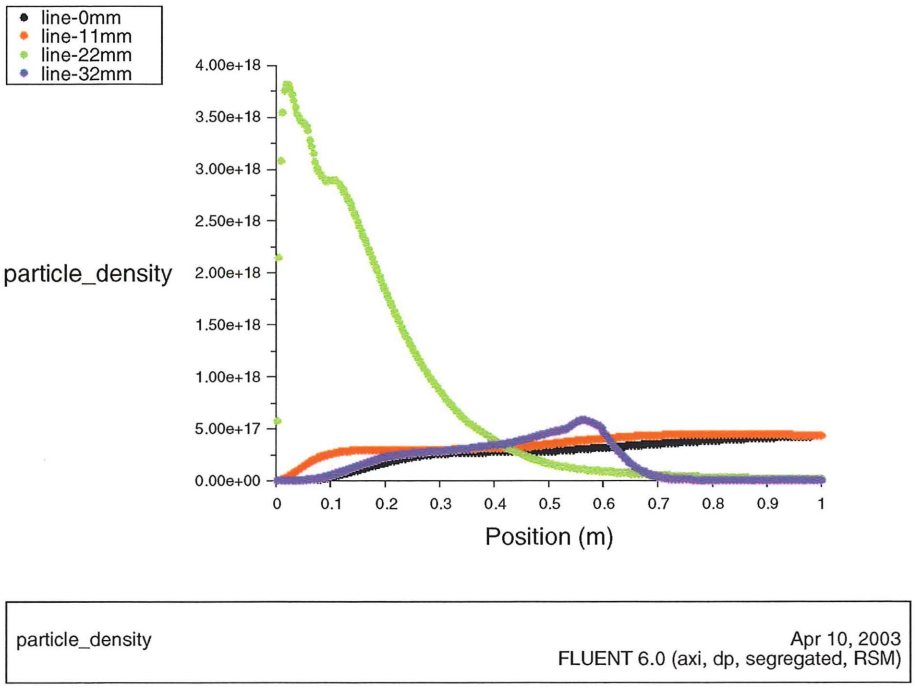

Figure 4.7: Particle concentration number - basic case

In the figure 4.7, the particle number concentration is shown for the basic case. The particle number concentration increases drastically from zero to about $1x10^{19}[\sharp particles/m^3]$ at the entrance of the reactor. The increase becomes stable around 60 cm of the axis, mainly near the axis. Here the concentration is maintained about $1x10^{17}$. As the gas passes along the reactor, coagulation starts to take place and to reduce the particle number density, as shown mainly by lines near the wall. The coagulation rate increases with the concentration of particles. However, when the temperature of the gas is lower than the melting point of the metal, particles are in solid state and collisions among them may occur while the particles cannot coalesce.

The particle number concentration is zero at the wall because particles cannot exist at this point. Inside the reactor, the concentration of particles is high near the injection, where these are formed by nucleation, and then it decreases by coagulation as the particles go along the reactor. Towards the end of the reactor, the concentration profiles are quite flat.

Isocontours of the concentration of iron particles are given next for the other two cases studied.

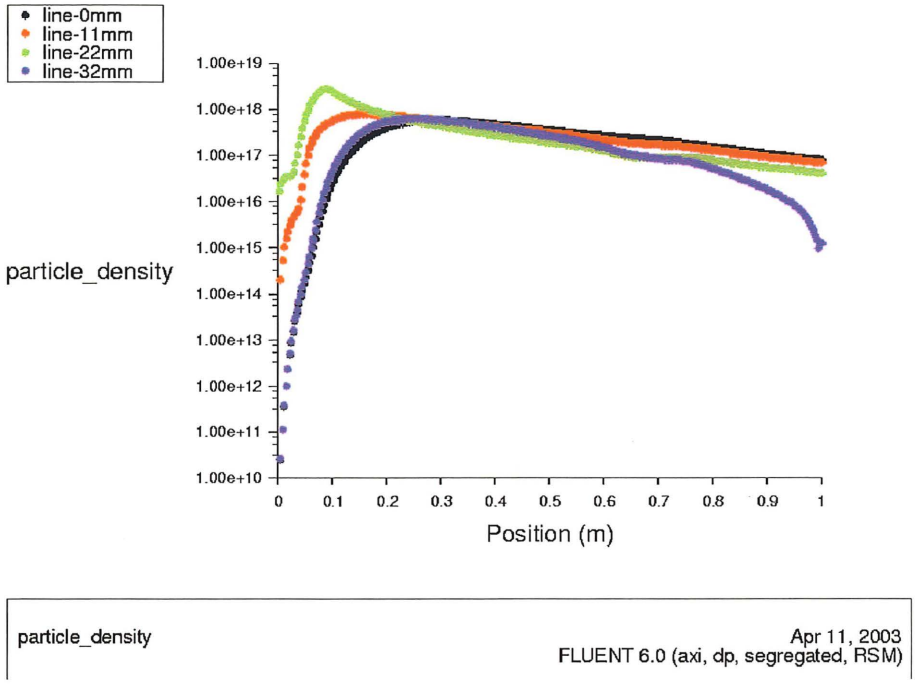

Figure 4.8: Particle concentration number - without quenching

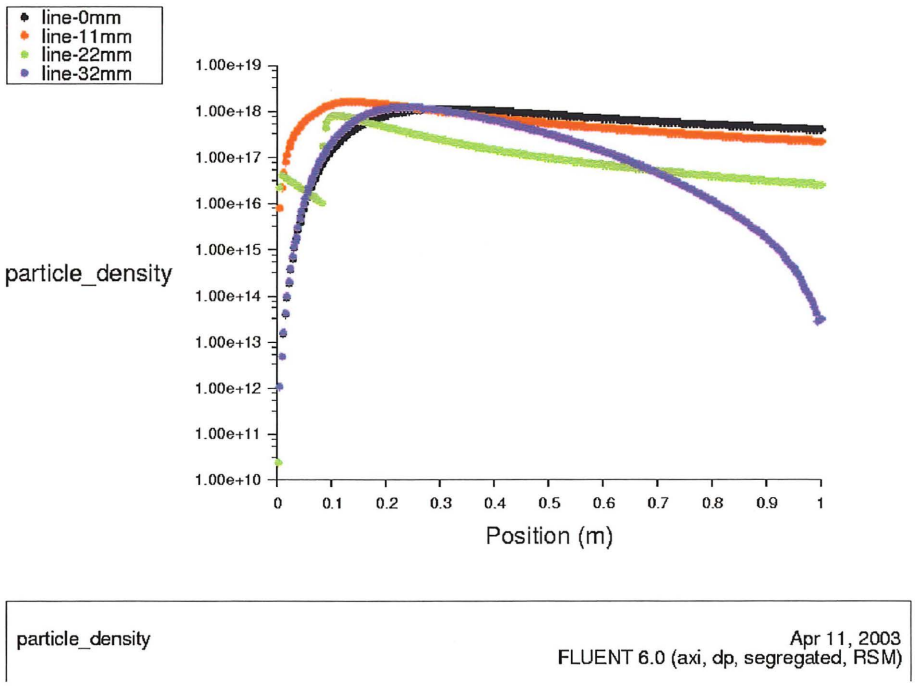

Figure 4.9: Particle concentration number - quenching 236 lpm

Figures 4.8 and 4.9 show that high particle concentrations are formed near the entrance of the reactor wall. This is due to the strong-temperature gradients and thus the little time available for growth. Particle deposition along the length of the induction zone, mainly due to thermophoresis, typically accounts for 10 percent of the initial metal feedrate. Important temperature gradients are also encountered directly below the step, causing the formation of high concentrations of particles. The particles are formed further downstream and in smaller concentrations on the reactor axis, due to the more gradual cooling. The particle cloud is gradually deviated towards the reactor axis due to the injection of gas through the wall.

Particle mean diameter

Figures 4.10, 4.11, and 4.12 are representative of the particle mean diameter behavior across the reactor.

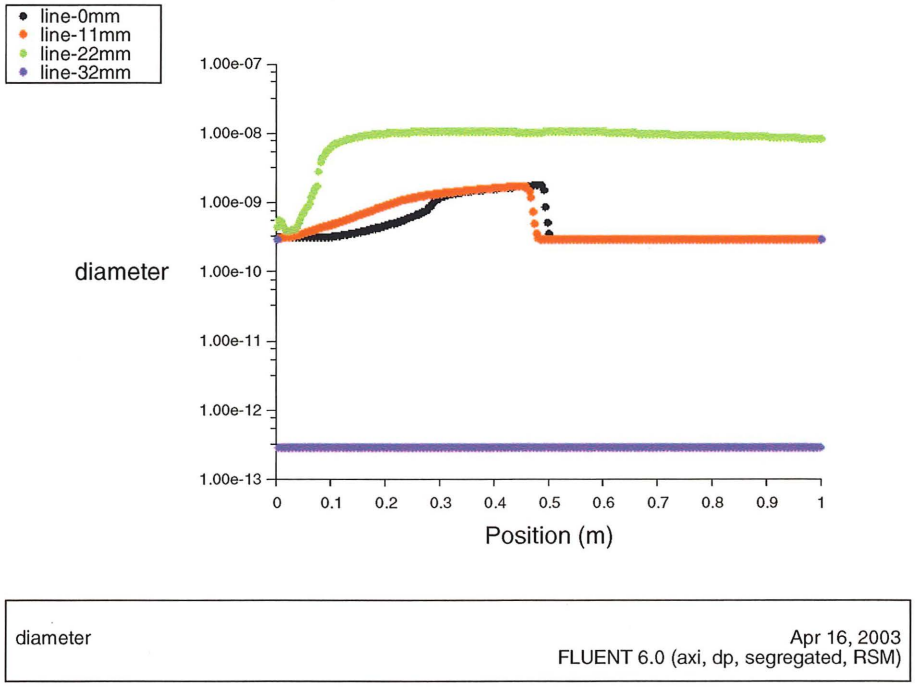

Figure 4.10: Diameter of particles - basic case

It is observed how the particle mean diameter is affected by nucleation, condensation and coagulation. At the entrance of the reactor, nucleation takes place near the wall, there after the particles grow by condensation and coagulation. Once the particles reach the injection zone of quenching, the temperature of the gas drops dramatically and the saturation ratio increases giving rise to a nucleation location. At this point many

particles of critical cluster size are formed and a sudden increase in the geometric mean diameter is observed.

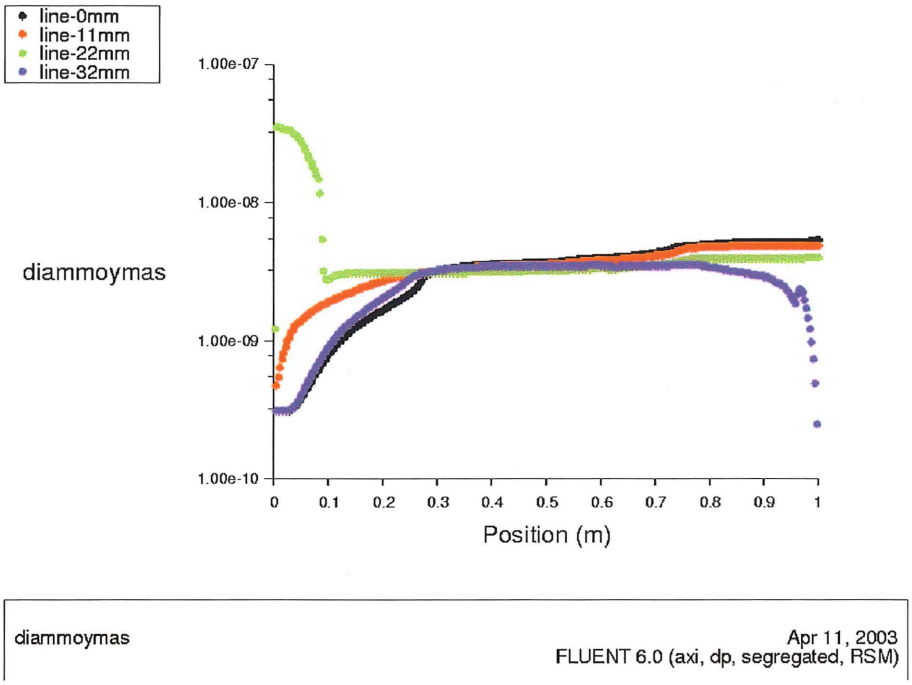

Figure 4.11: Diameter of particles - without quenching

After quenching injection, the already existing particles start to coagulate and to form bigger particles, increasing the particle geometric mean diameter of the size distribution function. This is clearly observed on line-22mm which is near the wall of quenching. Condensation on the existing particles also occurs after the injection quenching helping to increase the size of the particles.

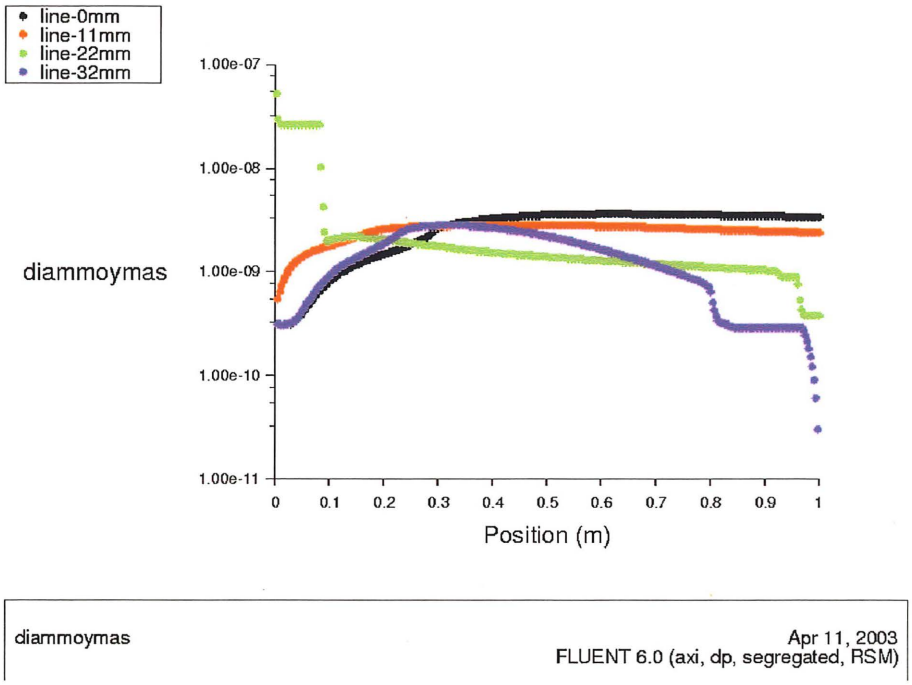

Figure 4.12: Diameter of particles - 236 lpm

Geometric standard deviation

Results let see that at the entrance of the reactor the standard deviation is relatively low because at this point new particles are formed at a unique size. However, the particles start to coagulate and the condensation of more material on the surface increases the size of particles. The formation of new particles of only one size results in a standard deviation of one, monodisperse aerosol, at this spot. However this value is changed by further nucleation and diffusion of particles, making the aerosol polydisperse. It is appreciated in figures 4.13 to 4.14 and 4.15 for different quenching rates.

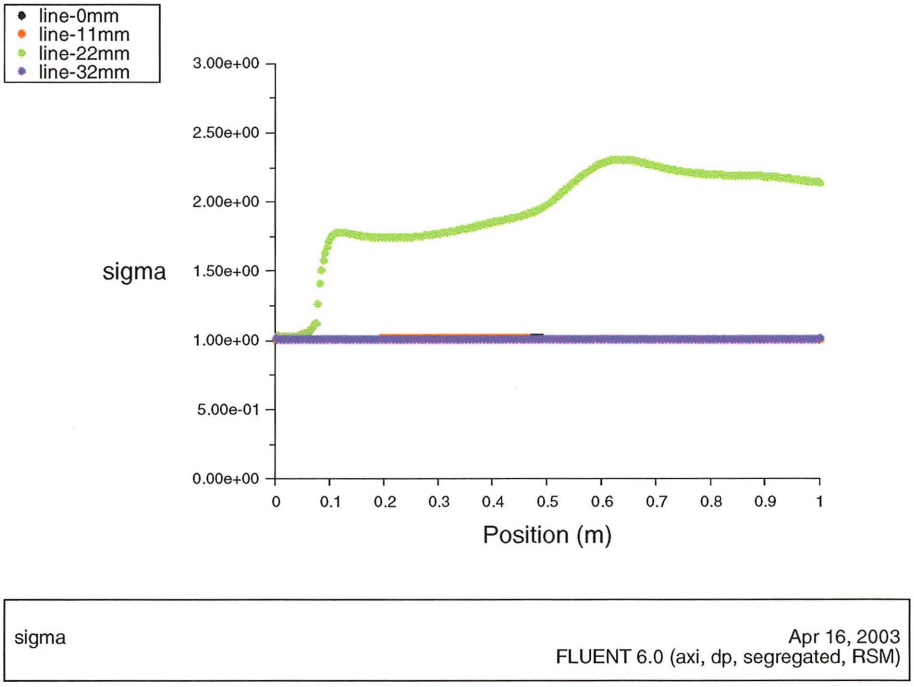

Figure 4.13: Geometric Standard Deviation-without quenching

At the quench injection, the formation of new particles increases the geometric standard deviation of the particles. The existing particles were generated at the nucleating site, and which becomes stable along the reactor; therefore the standard deviation of the size distribution becomes stable also. This point, hold the main assumption of the model, that the particle size distribution is fully described by a lognormal distribution function with only one mode.

The lognormal distribution function is usually used because is an approach inspired by typical pictures of measured particle size distribution [47].

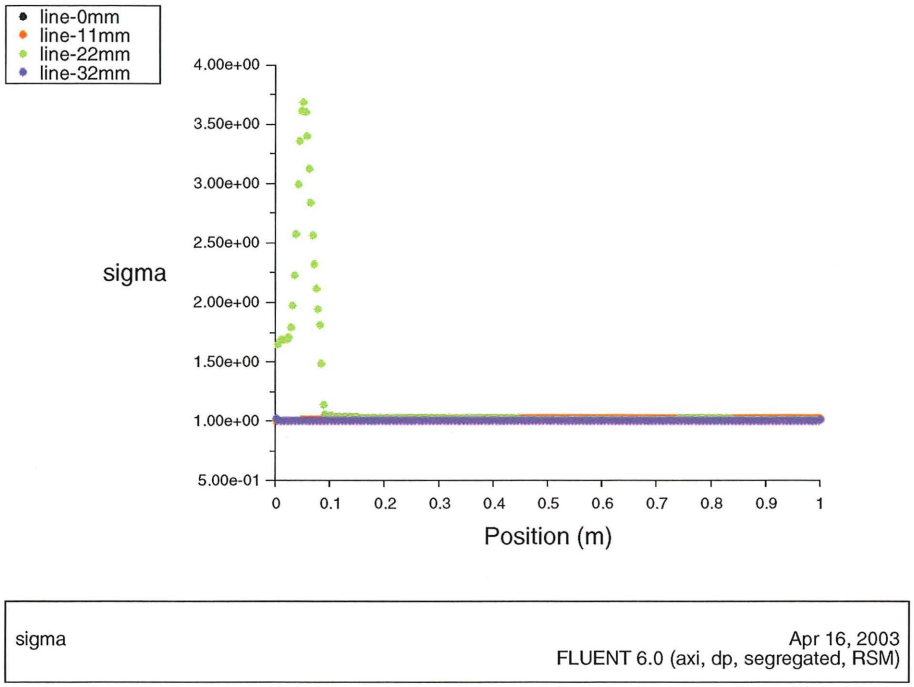

Figure 4.14: Geometric Standard Deviation-quenching 118 lpm

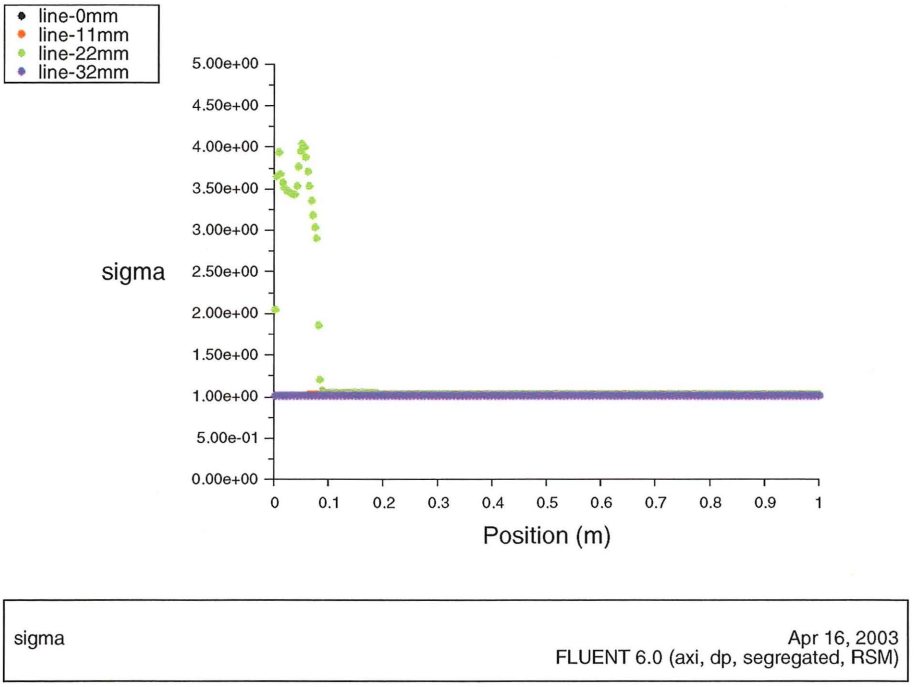

Figure 4.15: Geometric Standard Deviation-quenching 236 lpm

4.2.2 Influence of metal vapor concentration on the nanoparticle growth

Increasing the concentration of metal in the gas phase increases the amount of material being processed per unit time, increasing productivity. On other hand, decreasing the metal vapor concentration may favor the production of certain desired types of particles. The study of the effect of the metal vapor concentration on the particle properties has been carried out the results presented below.

Particle number concentration

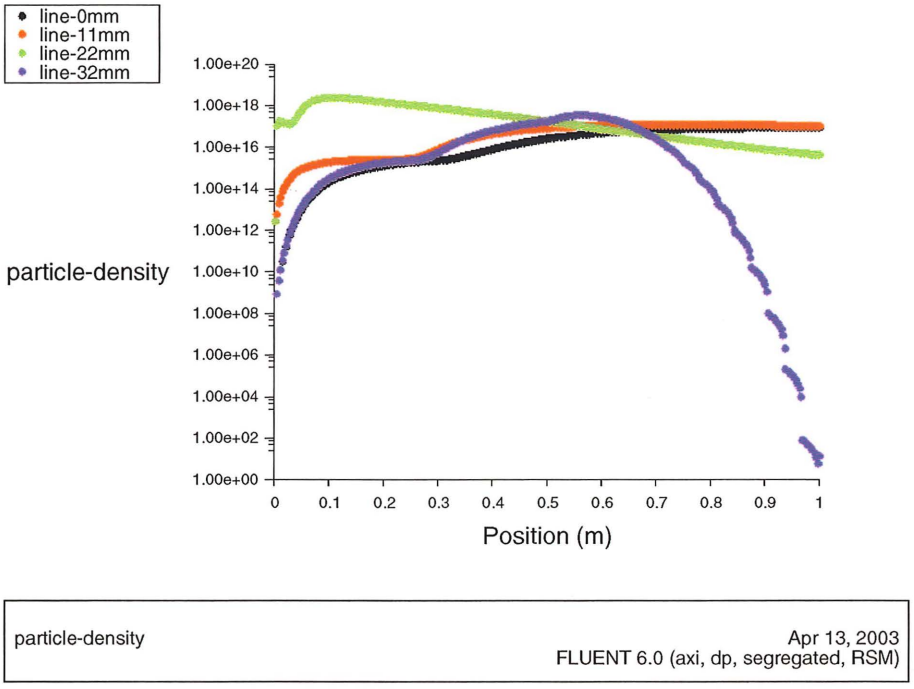

Figure 4.16: Particle number density-iron concentration = $1x10^{-4}$ $[kg_{Fe}/kg_{Ar}]$

In figures 4.16, 4.17, and 4.18 the axis representing the particle number concentration is in a logarithmic scale to clearly represent the fast increasing of this property. It is shown that the particle number concentration increases at the lower end as the metal vapor concentration is increased due to the increase in the condensable material introduced in the reactor. Due to the low concentration of metal vapor, the entrance nucleation wakens and the great majority of the particles are produced at the entrance point, where the low temperature of the quenching gas induces the nucleation of particles. As the concentration increases the amount of material nucleated increases until it reaches the point where the entrance nucleation becomes important. In fact, nucleation and condensation are competitors for the available metal atoms in the gas phase to form condensed material; therefore condensation may suppress nucleation. This suppression

is responsible for the decrease of the particle number concentration as the metal vapor concentration increases.

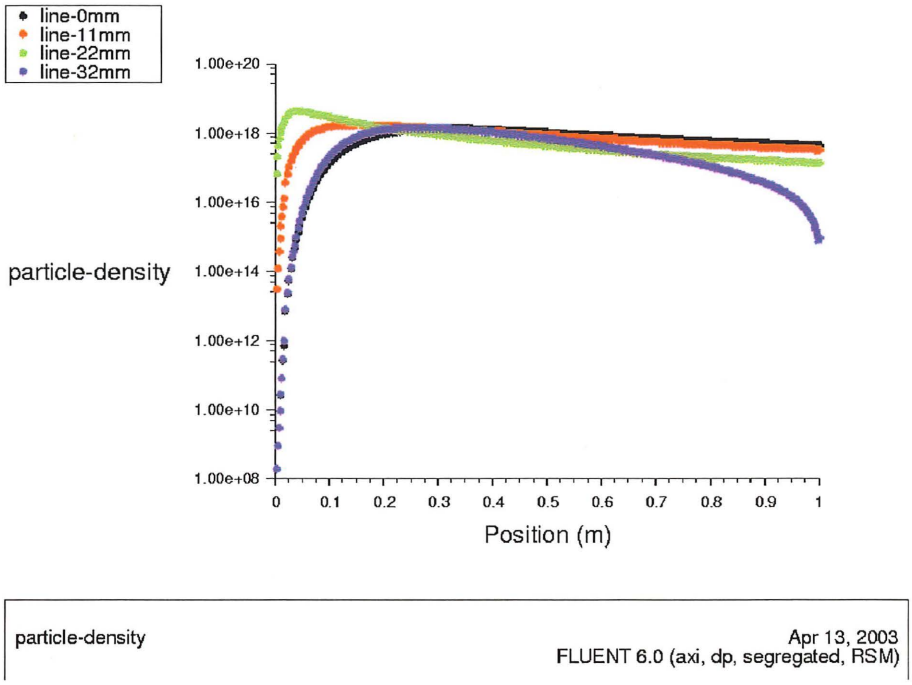

Figure 4.17: Particle number density-iron concentration = $1x10^{-5}$ $[kg_{Fe}/kg_{Ar}]$

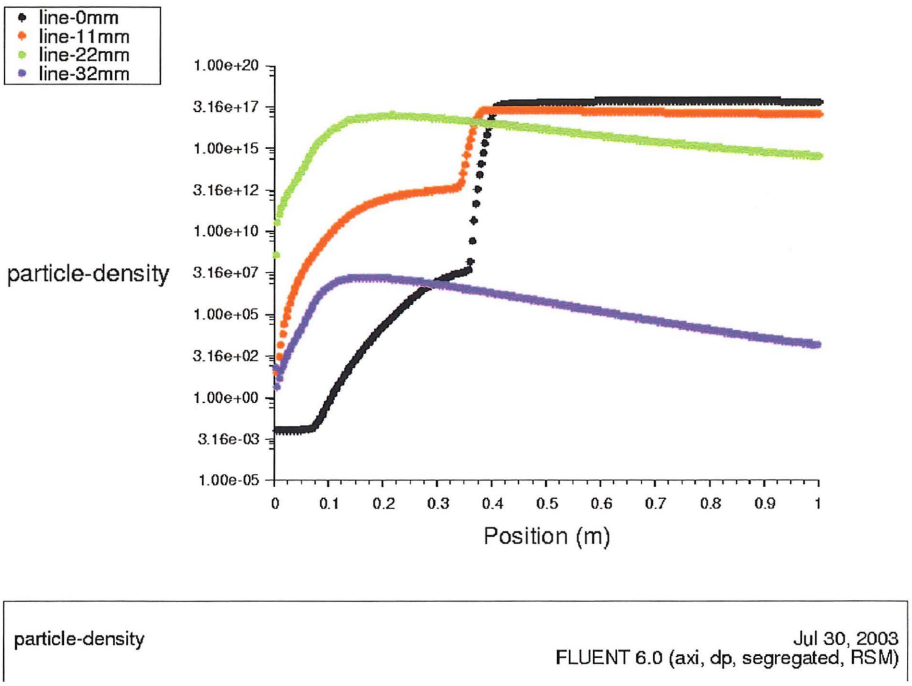

Figure 4.18: Particle number density-iron concentration = $1x10^{-6}$ $[kg_{Fe}/kg_{Ar}]$

Particle mean diameter

The particle size increases as the amount of condensable metal in the reactor is increased since the concentration of particles is high enough for coagulation to increase the particle geometric mean diameter.

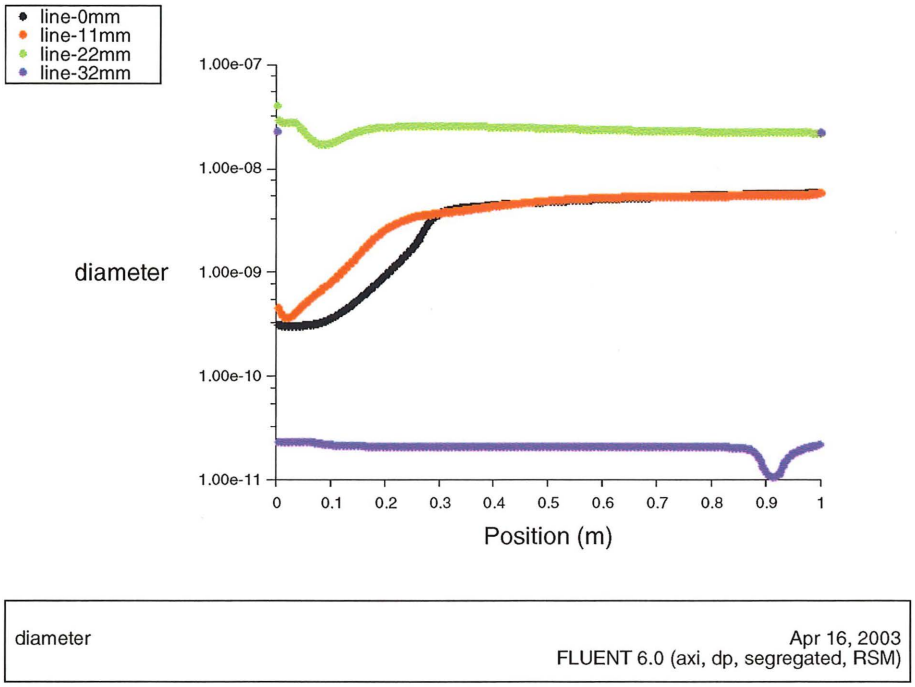

Figure 4.19: Diameter-iron concentration = $1x10^{-4}$ $[kg_{Fe}/kg_{Ar}]$

Figures 4.19, 4.19, and 4.19 refer different values of mean diameter of particle for three different iron concentration cases. If they are compared, it is noted that size of particles are more uniform for low concentrations. The best size of particles is found in he case of lowest iron concentration: $1x10^{-6}$ $[kg_{Fe}/kg_{Ar}]$

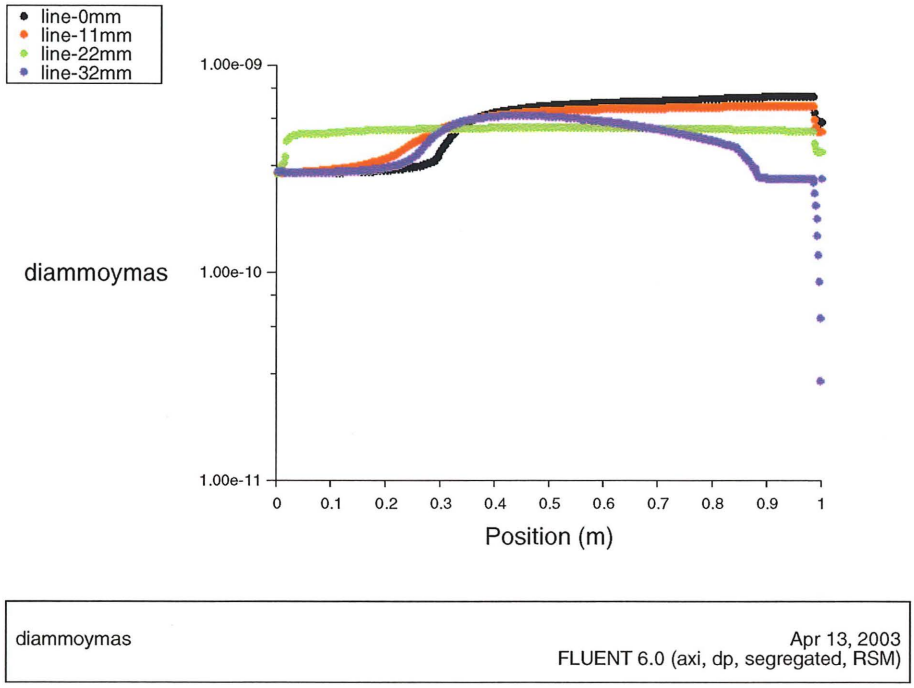

Figure 4.20: Diameter-iron concentration = $1x10^{-5}$ $[kg_{Fe}/kg_{Ar}]$

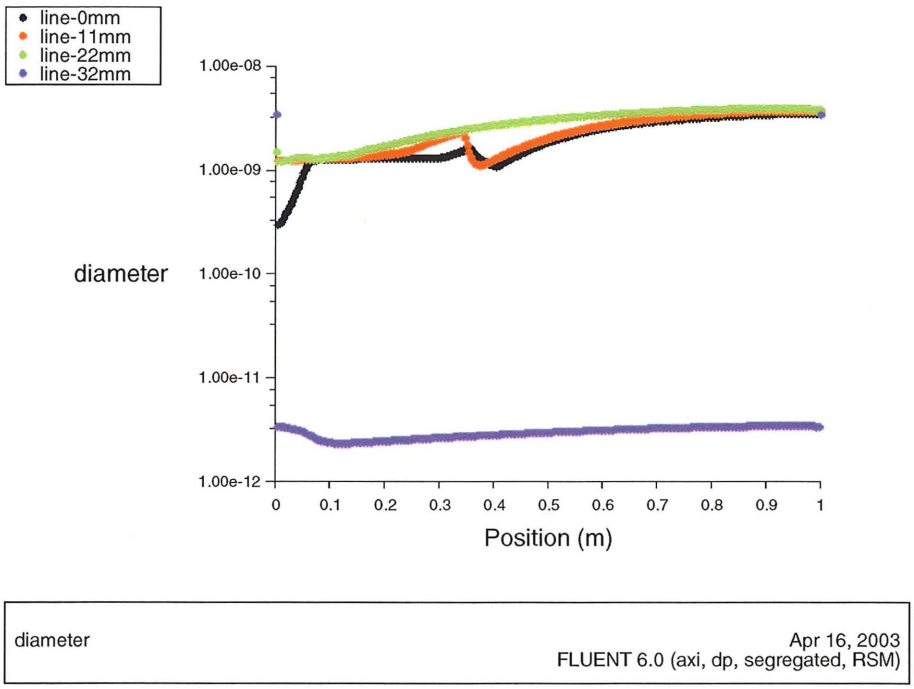

Figure 4.21: Diameter -iron concentration = $1x10^{-6}$ $[kg_{Fe}/kg_{Ar}]$

Geometric standard deviation

The geometric standard deviation is also affected by changes in the metal vapor concentration. Intuitively an increase in the standard deviation would be expected as the metal vapor concentration increases since this produces higher density of particles as observed in figure 4.22. However, the figure 4.23 shows how the opposite happens.

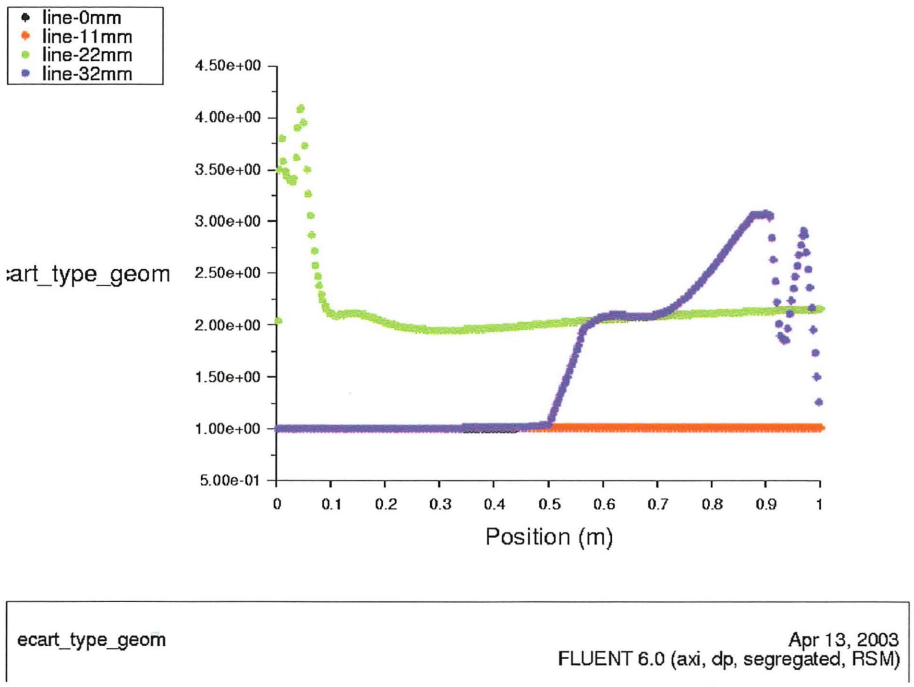

Figure 4.22: Geometric standard deviation-iron concentration = $1x10^{-4}$ $[kg_{Fe}/kg_{Ar}]$

An uniformity of particle size is observed in the three cases, mainly in figure 4.23. In figure 4.22, the geometric standard deviation is uniform, 10 cm after the enter of the reactor, as shown in figure 4.21, which is considered as normal feature in the nanoparticle growth.

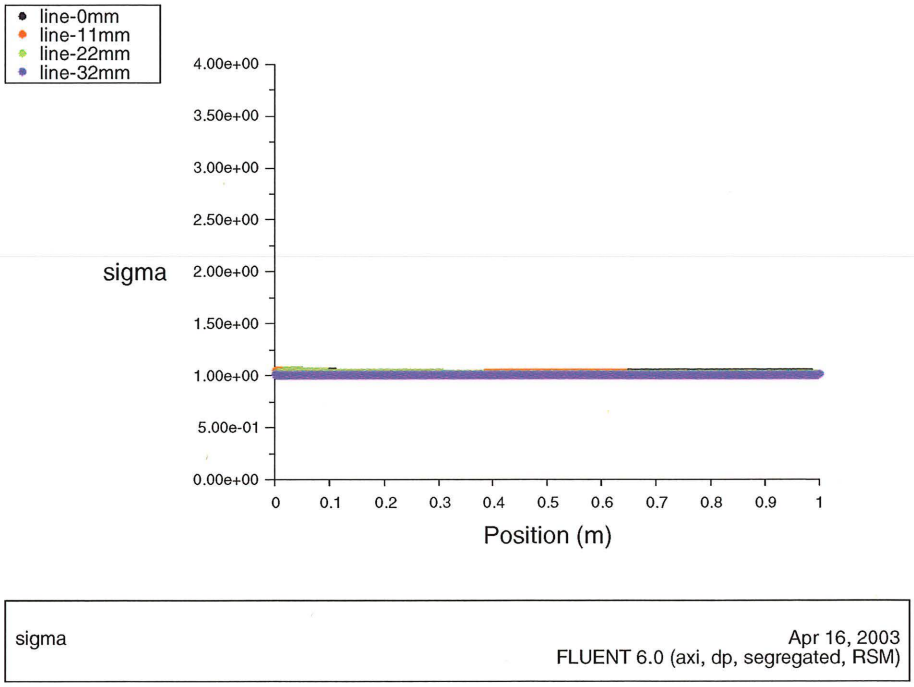

Figure 4.23: Geometric standard deviation-iron concentration = $1x10^{-5}$ $[kg_{Fe}/kg_{Ar}]$

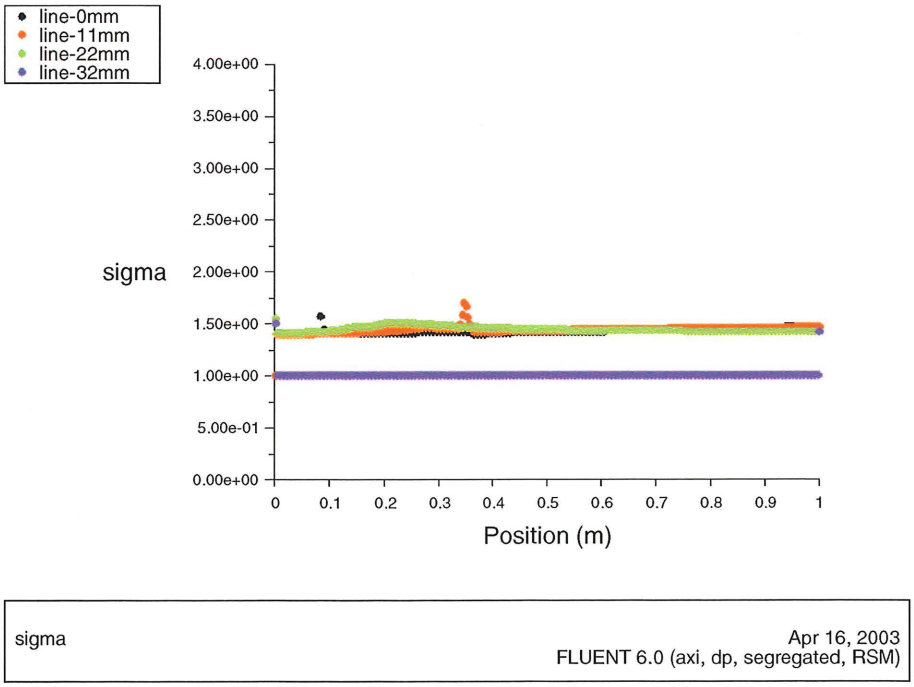

Figure 4.24: Geometric standard deviation-iron concentration = $1x10^{-6}$ $[kg_{Fe}/kg_{Ar}]$

4.3 Analysis of different quenching injection design

According last analysis, the quenching rate is very important in the process of nanoparticle growth. This quenching influences a lot the size and uniformity of particles produced. The quenching design method used for the cases presented in chapter 3, was a lateral injection over the entire wall of the reactor as shown in figure 4.26:

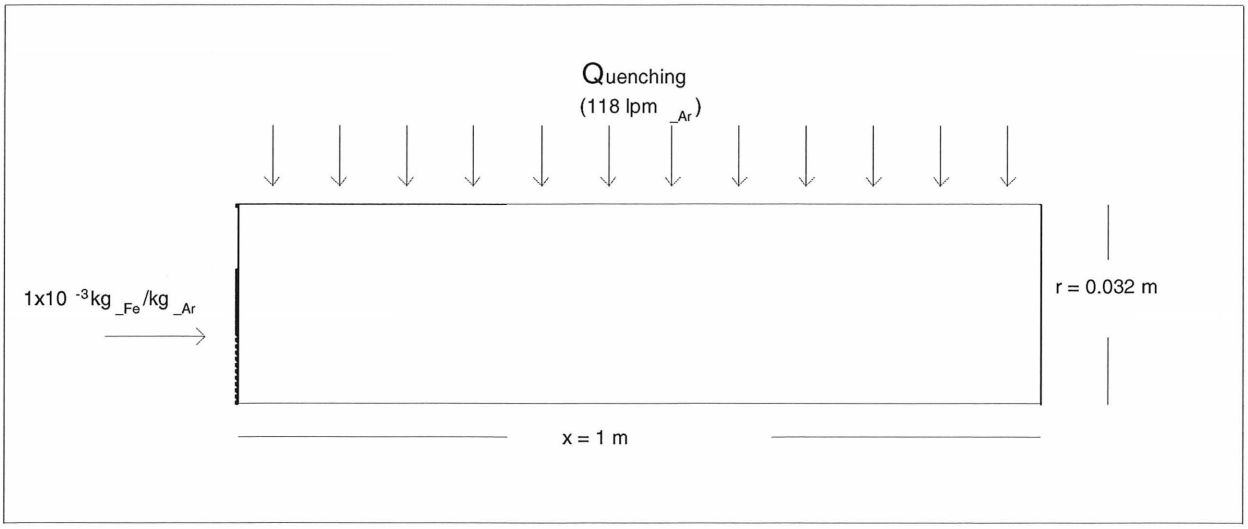

Figure 4.25: Quenching design: entire wall of the reactor

Results were found satisfactory. For this project it was considered interested to check what happen if is only used a fraction of the entire wall as quenching entrance. Next section proposes 3 different sections for injecting the quenching rate. The effect of the injection angle is also presented in the last part. An evaluation of the main nanoparticle properties is presented in each case.

4.3.1 Lateral injection covering 1/3 of the reactor wall

The same geometry described in Chapter 3 was used for this situation. For modifying the quenching section in the simulation software, only a change in the boundary condition of the control panel of the Fluent solver was required. It means, the porous zone before specified as boundary inlet, was split in three parts. In this section, the first part remained as velocity inlet, the two others as wall boundary. It is shown better in the next figure 4.26:

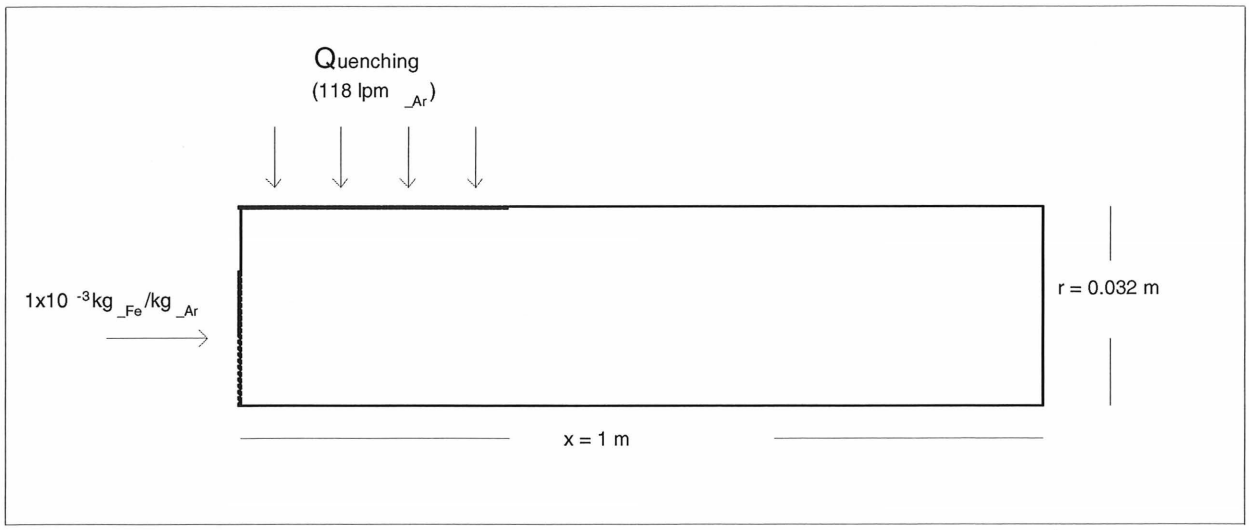

Figure 4.26: Quenching design: 1/3 of the reactor wall

The lateral injection over the 1/3 part of the reactor represents a smaller section of cooling for the iron vapor compared to the basic case before presented. However, it was enough to quench the vapor and to produce a successful nucleation of particles. Results below, show the temperature, vapor concentration, mean diameter and the geometric standard deviation obtained for this case.

Temperature values registered on the first 30 cm of the reactor are high for almost all radial section. A following decreasing is observed as result of quenching and temperature of the wall.

The particle number density is increased not as faster as observed in the basic case (fig. 4.7). However, it is more similar for all radial positions excepting at the wall.

Figure 4.27 shows big particles near the wall and smaller ones near the axe.

A satisfactory value of the geometric standard deviation is observed in figure 4.28. That means there is an uniformity in the particle size distribution of particles.

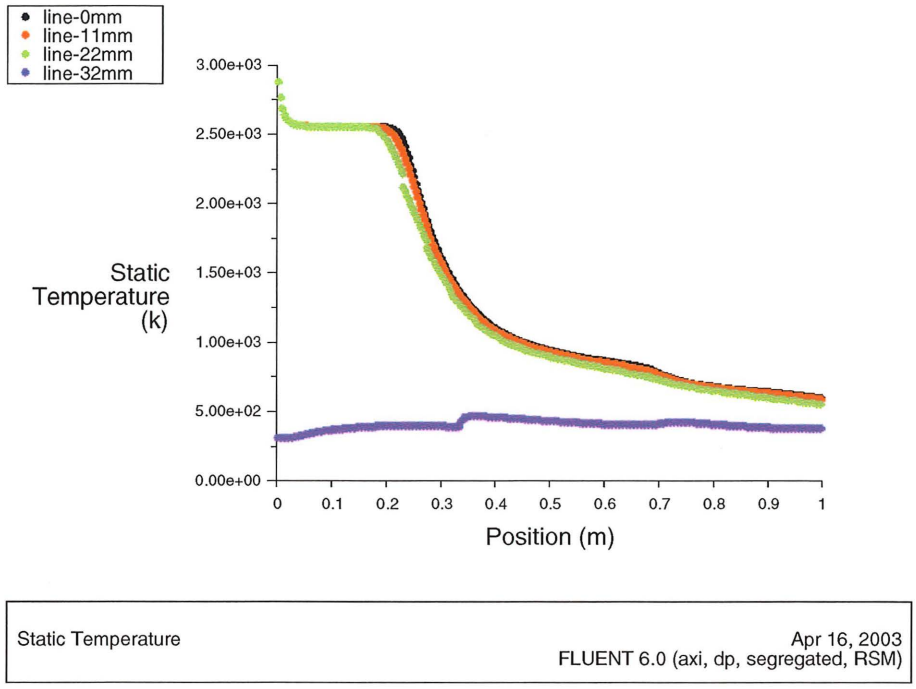

Figure 4.27: Xy plot of temperature - quenching section: paroi2

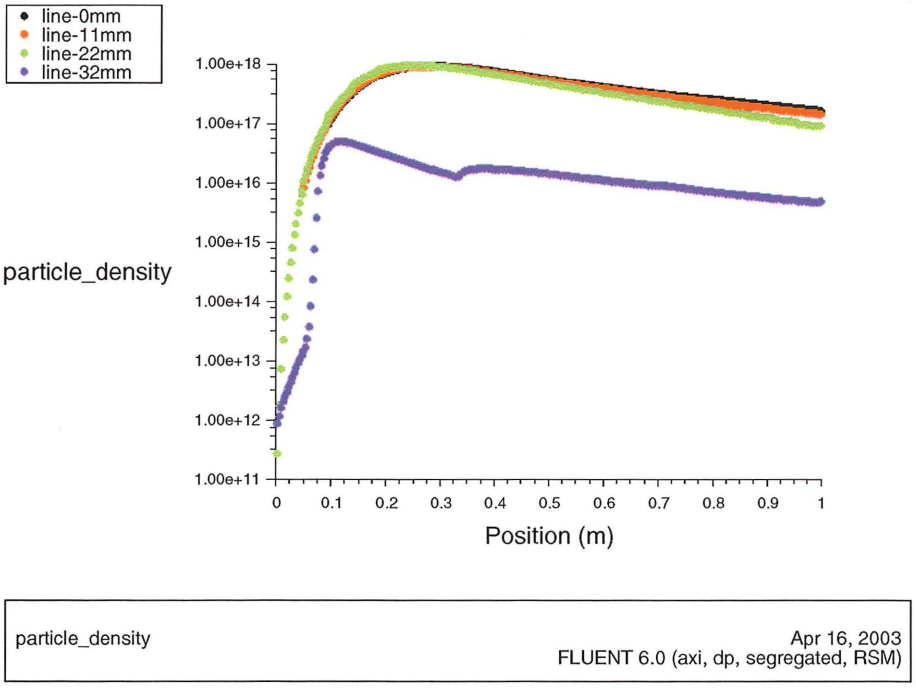

Figure 4.28: Particle number density - quenching section: paroi2

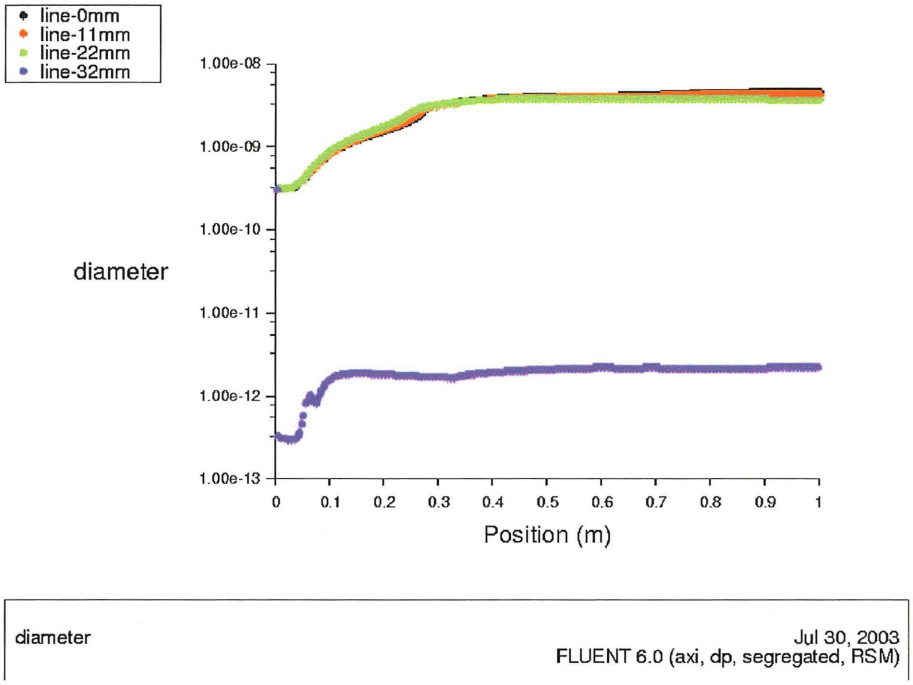

Figure 4.29: Mean diameter - quenching section: paroi2

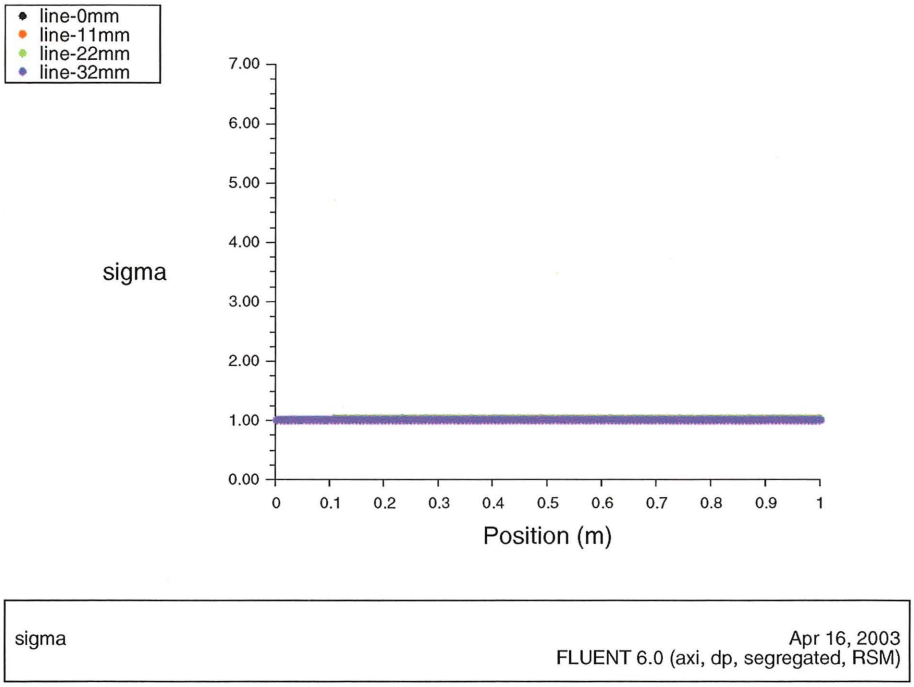

Figure 4.30: Geometric standard deviation - quenching section: paroi2

4.3.2 Lateral injection covering 2/3 of the reactor wall

The quenching section is longer compared to the case before presented. The figure 4.31 below is provided for a better understanding of the physical injection of the quench.

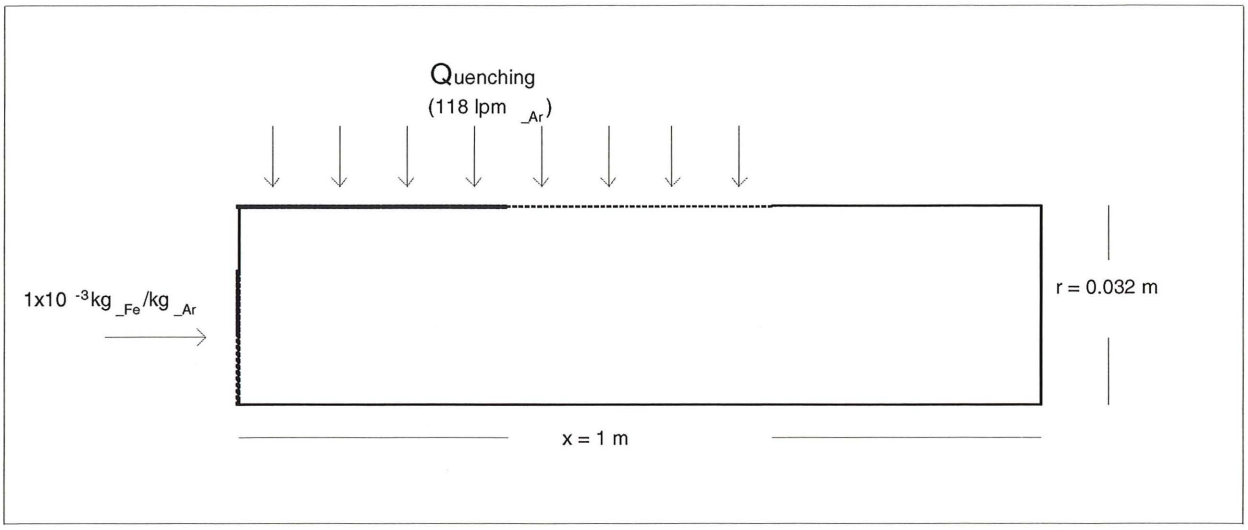

Figure 4.31: Quenching design: 2/3 of the reactor wall

The quenching injection over the 2/3 of the reactor wall acted efficiently producing the nucleation burst of particles. This is reflected in the sudden temperature decreasing at 30 cm of the long of the reactor, as shown in figure 4.32.

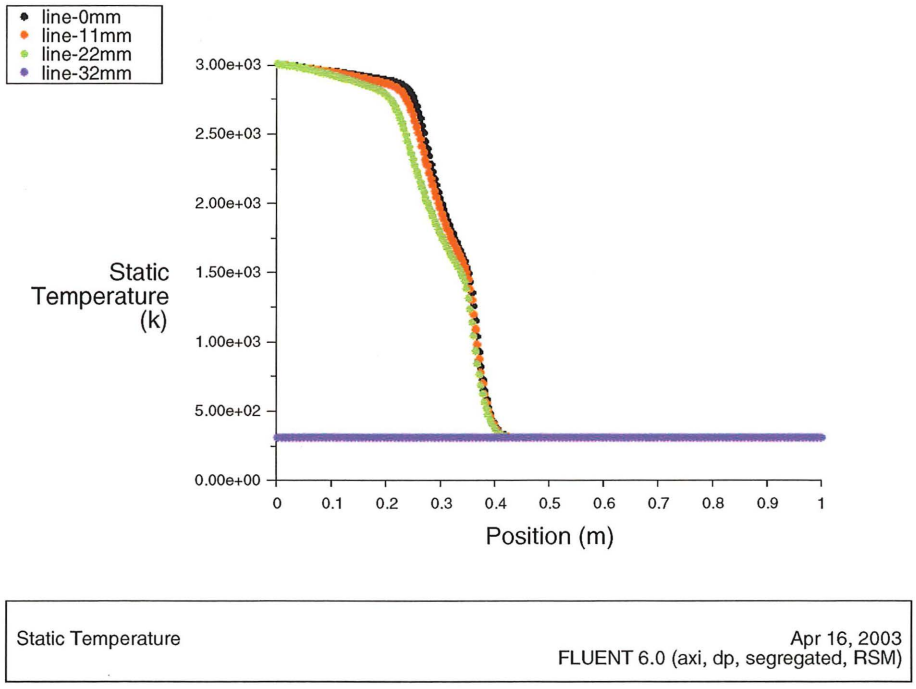

Figure 4.32: Xy plot of temperature - quenching section: paroi2 et paroi3

Particle number density is increased since the enter of the mass flow rate to the reactor. Figure 4.33 shows how the maximum value is reached around 20 cm after the entrance. The uniformity of the particle number density finish at 60 cm when it is decreased near the wall.

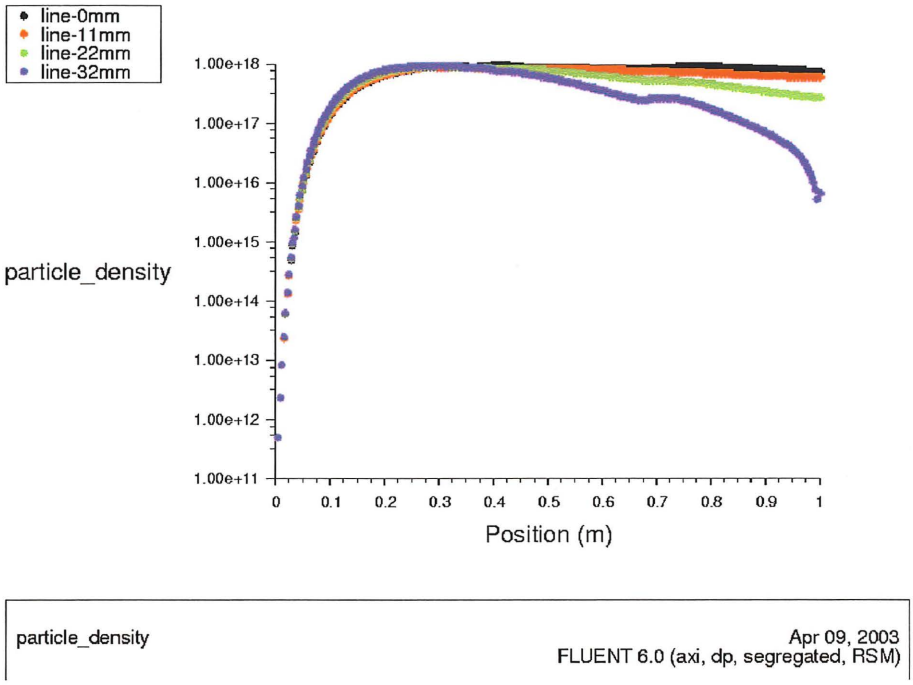

Figure 4.33: Particle number density - quenching section: paroi2 et paroi3

The effect of the quenching over the size of particles is observed in figure 4.34. Values for the diameter of particles are smaller compared to the last case. It means that increasing of quenching section helps the production of smaller particles.

Figure 4.35 allows to appreciate the good uniformity of particle sizes with values of the geometric standard deviation near to one.

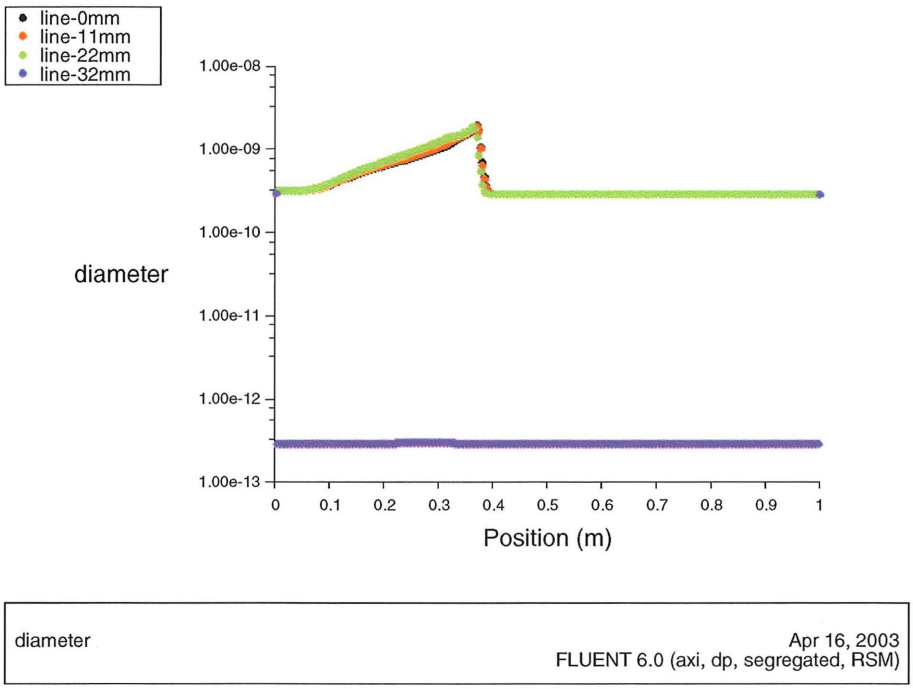

Figure 4.34: Mean diameter - quenching section: paroi2 et paroi3

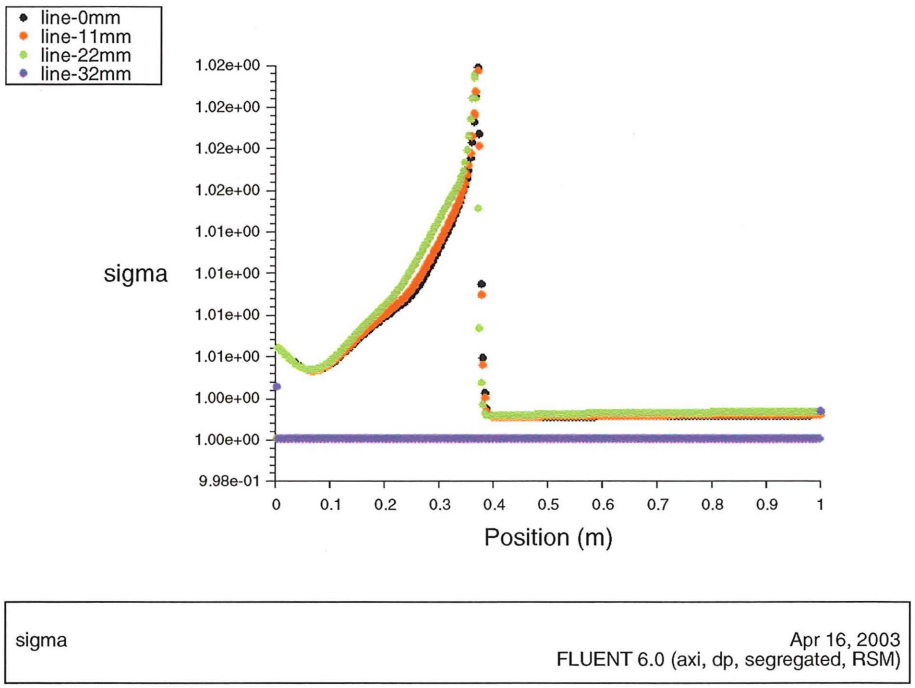

Figure 4.35: Geometric standard deviation - quenching section: paroi2 et paroi3

4.3.3 Angular injection rate

Designs of quenching presented before are related because they act on the wall zone of the reactor. It means, the wall was always adapted with modifications to allows the quenching acting in different positions (1/3 and 2/3 of the wall). This section suggests a different design. An angular injection quenching of 45 degrees accounting for the axial position of the wall besides the entrance of the mass flow rate, was tried. The figure 4.36below represents this design.

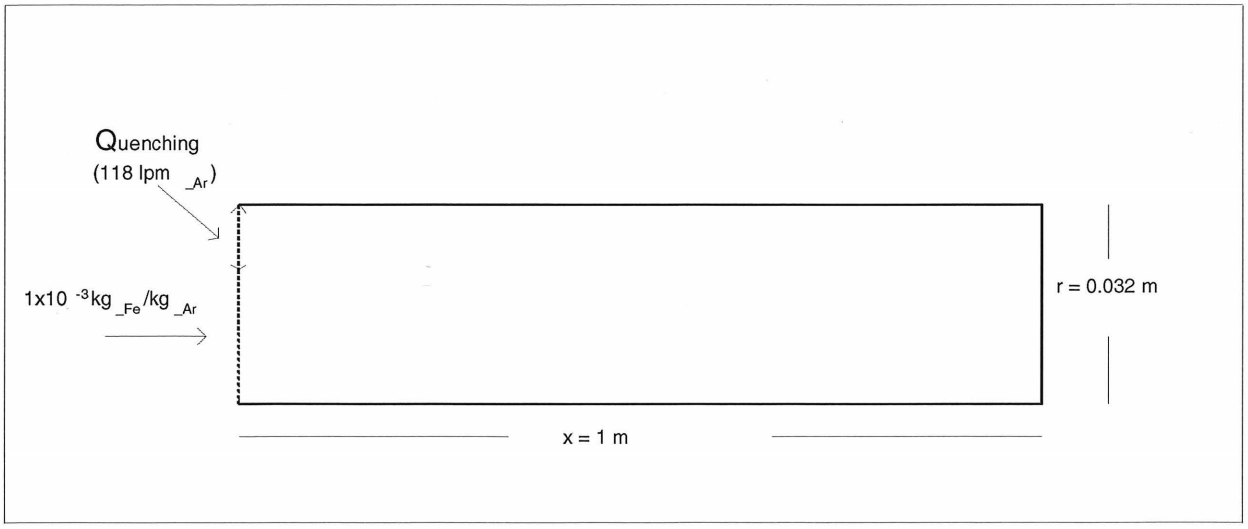

Figure 4.36: Quenching design: angular quench

Results are shown below.

Different temperature profiles to those of last part are obtained. Figure 4.37 shows how near the axe, temperature decreases slowly. Nevertheless, near the wall of the reactor the decreasing is very fast.

Interesting values of particle number density are observed in figure 4.38. Near the axe, there is a high increasing of $1x10^{20} \sharp particles/m^3$, even higher other analyzed cases. It is important to note that there is a god number concentration near the wall.

The diameter of particles reported in figure 4.39 is extraordinary for the nanoparticles size requirements of 10 to 100 nanometers. The geometric standard deviation predicts a good uniformity in the particle distribution size.

It is important to consider that the quenching flow rate was maintained constant, with the value of the basic case, 118 lpm. All other parameters were also those of the basic case.

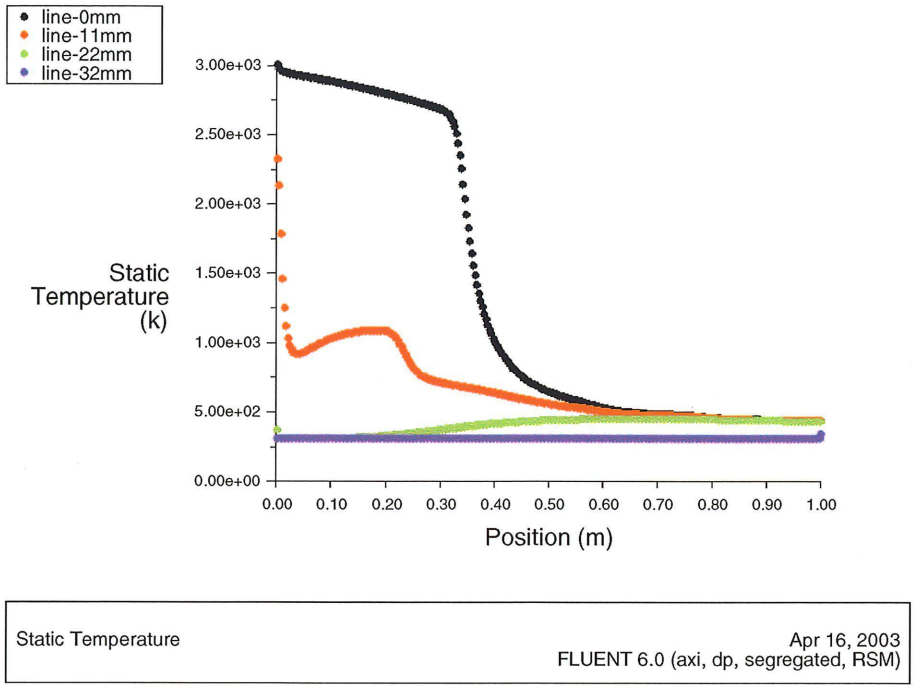

Figure 4.37: Xy plot of temperature - quenching section: paroi2 et paroi3

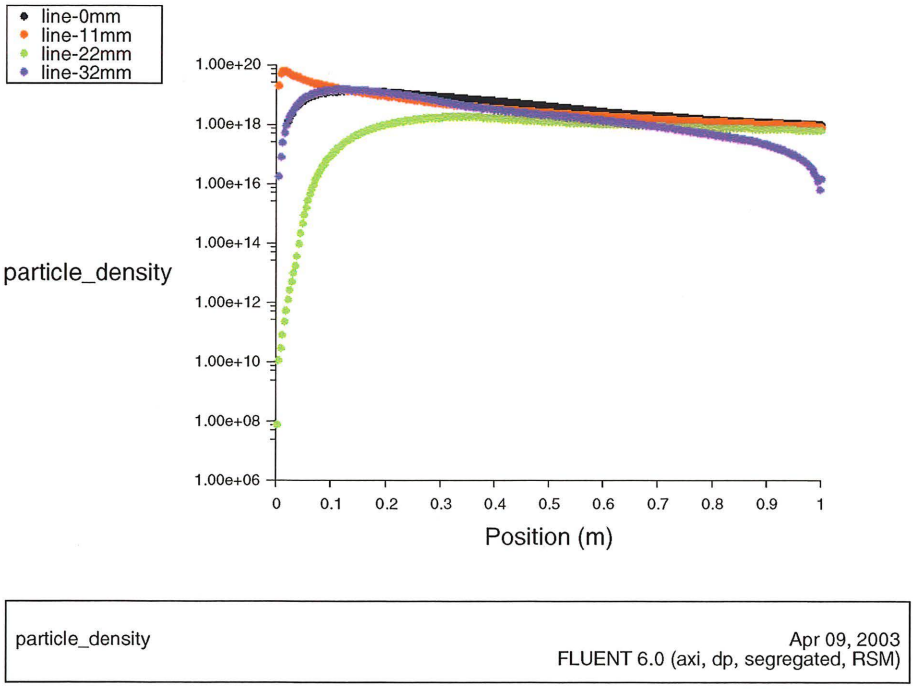

Figure 4.38: Particle number density - quenching section: angular section

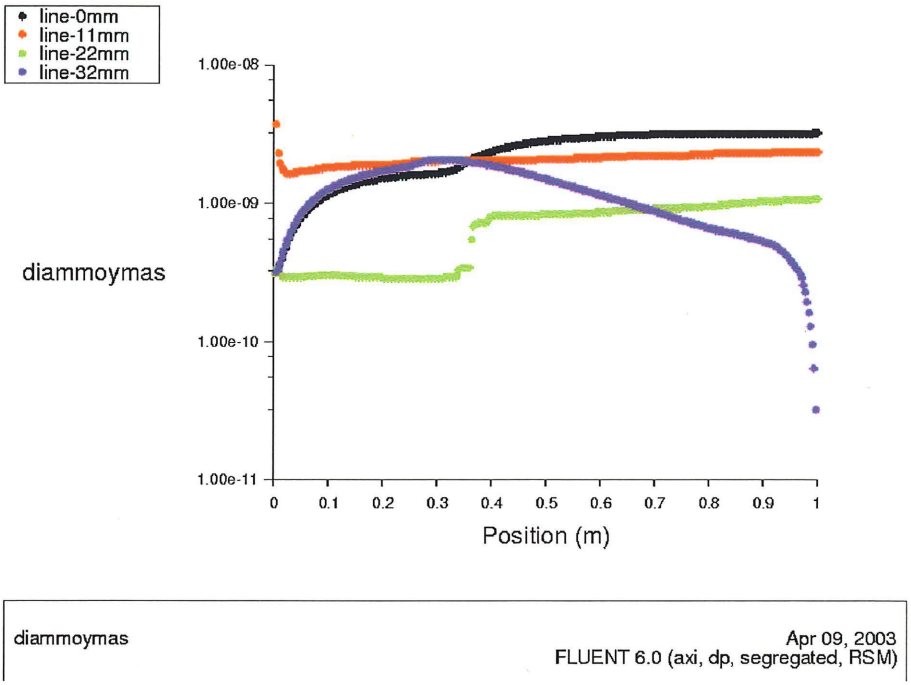

Figure 4.39: Mean diameter - quenching section: angular section

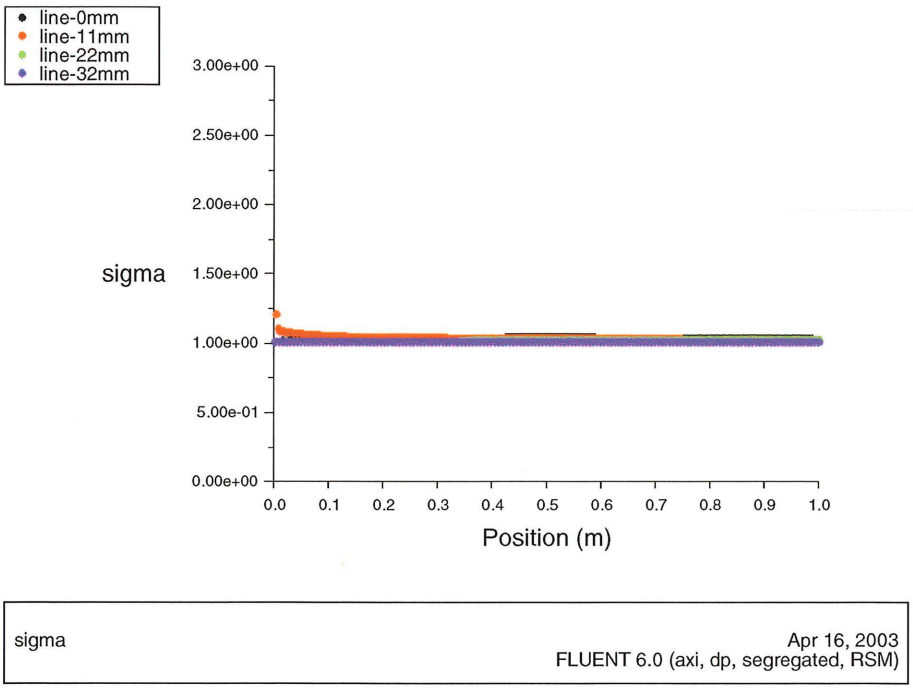

Figure 4.40: Geometric standard deviation - quenching section: angular section

Chapter 5

CONCLUSIONS AND FUTURE WORK

A CFD model of a particle generator with radial injection of a quenching gas has been developed to gain a better understanding of the process. The evolution of the particle size distribution wasbn calculated using the method of moments and assuming a lognormal particle size distribution.

A main step in the realization of this work was to introduce the equations of aerosol growth into the commercial software of CFD FLUENT©.

The model predicts the presence of a recirculation zone induced by the quenching rate. Turbulence is introduced into the reactor by the quenching flow rate. This quenching reduces the temperature of the gas from 3000 K to about 500 K. This decrease in temperature is important since it increases the saturation ratio of metal vapor giving rise to homogeneous nucleation of particles.

It was found that nucleation of particles depends on the concentration of metal vapor in the gas and the temperature. Then, the concentration of the metal vapor decreases sharply close to 1800 K temperature, indicating condensation. The metal vapor concentration is decreased primarily by nucleation and condensation.

The particle characteristics were studied by analyzing the particle number concentration, mean geometric diameter and the geometric standard deviation.

The effects of the following process parameters on the characteristics of the product were studied: injection flow rate and metal vapor concentration. With increasing injec-

tion rate, the particle mean diameter decreases while the geometric standard deviation increases slightly. Moreover, it was found that at high injection rates, the amount of product recovered increases while the particle characteristics are relatively insensitive to the injection rate. This suggest that operating in the turbulent regime would be more efficient and insensitive to slight fluctuation in injection rate. The injection rate is one of the most important process parameters since it can be easily changed. Large particles or small particles can be produced just by adjusting the position of a valve.

It was found that changing the metal vapor concentration changes the governing mechanisms that affect the particle size distribution. Three different regions were identified. At low metal vapor concentration, low concentration of very small particles are obtained. Even though these particles are almost monodisperse, and it can't be easy to recover the material. It makes economically unattractive.

Three different designs of quenching injection section were analyzed. Results show an excellent agreement for the case of the angular quench injection.

It is important to note that the present model assumes that coagulation is not affected by the presence of turbulence in the reactor, since the particles being studied are in the free molecular regime. In this regime coagulation is mainly determined by brownian motion of the particles and the atoms in the gas rather than by turbulence interaction.

A partial comparison of calculated results with those of Bilodeau [1] was done in the order to validate the numerical model. An agreement about the zones of the reactor, where particles are formed, was found. The values of main properties as velocity, temperature and mass fraction were compared with similar semblance. Some advantages to stand out about the new CFD model created, are about the friendly access to change the different parameters and the reduced time of solving.

In the other hand, it is important to note for the present model some limitations related the physics of the problem. The model is limited to particles in the free molecular regime and low metal vapor concentrations.

In order to extend the capabilities of the present model, other phenomena have to be taken into account: brownian coagulation and condensation in the continuum and slip regime, turbulent shear coagulation and the latent heat during nucleation and condensation. The results have shown that working at high metal vapor may be desirable.

Bibliography

[1] J.F. Bilodeau. Modélisation de la croissance de poudres ultrafines en réacteur à plasma thermique. Thèse de doctorat, Université de sherbrooke. 1994, 191 p.

[2] H. Gleiter. Nanostructured materials: basic concepts and microstructure control of nanoparticles. *Acta Mater*, 48:1–29, 2000.

[3] M.C. Roco. Nanoparticles and nanotechnology research. *Journal of Nanoparticle Research*, 1:1–6, 1999.

[4] T. Yoshida and K. Akashi. Preparation of ultrafine iron particles using an rf plasma. *Transactions of the Japanese Institute for Metals*, 22:371–378, 1981.

[5] W.L. Barmore, L.W. Hrubesh, L.E. Keene, and E.L Raymod. Induction plasma apparatus for generating submicron particles of metals. *Review of Scientific Instruments*, 60:1328–1332, 1989.

[6] S.L. Girshick, C.P. Chiu, R. Muno, C.Y. Wu, L. Yang, S.K. Singh, and P.H. Mcmurry. Thermal plasma synthesis of ultrafine iron particles. *Journal of Aerosol Science*, 24:367–382, 1993.

[7] A. J. Becker, T. N. Meyer, F. N. Smith, and J. F. Edd. Plasma process routes to synthesis of carbide, boride and nitride ceramic powders. *Materials Research Society Symposium Proceedings*, 98:335–346, 1987.

[8] C. B. Laflamme. Synthèse de poudres ultrafines de carbure de silicium dans un réacteur à plasma à courant continu.Thèse de doctorat, Université de sherbrooke. 1991, 151 p.

[9] G. Soucy. Synthèse de poudres ultrafines de si_3n_4 par plasma inductif. Thèse de doctorat, Université de sherbrooke. 1992, 233 p.

[10] S. Gutierrez. $MoSi_2$, Une nouvelle génération de matériau structural pour des applications haute température. Report of Predoctoral Exam, Université de Sherbrooke. 2001, 83 p.

[11] F. Gelbard and J. H. Seinfeld. Numerical solution of the dynamic equation for particulate systems. *J. Comput. Phys.*, 28:357–375, 1978.

[12] F. Gelbard and J. H. Seinfeld. The general dynamic equation for aerosols:theory and applications to aerosol formation and growth. *J. Colloid Interface Sc.*, 68:363–383, 1979.

[13] F. Gelbard and J. H. Seinfeld. Simulation of multicomponent aerosol dynamics. *J. Colloid Interface Sc.*, 78:485–501, 1980.

[14] F. Gelbard, Y. Tambour, and J. H. Seinfeld. Sectional representations for simulating aerosol dynamics. *J. Colloid Interface Sc.*, 78:541–556, 1980.

[15] S.L. Girshick, C.P. Chiu, and P.H. McMurry. Modelling particle formation and growth in a plasma synthesis reactor. *Plasma Chemistry Plasma Processing*, 8:145–157, 1988.

[16] S.L. Girshick and C.P. Chiu. Homogeneous nucleation of particles from the vapor phase in thermal plasma synthesis. *Plasma Chemistry Plasma Processing*, 9:355–369, 1989.

[17] S.V. Joshi, Q. Liang, J.Y. Park, and J.A Bardorf. Effect of quenching conditions on particle formation and growth in thermal plasma synthesis of fine powders. *Plasma Chemistry Plasma Processing*, 10:339–358, 1990.

[18] P. Proulx and J.F. Bilodeau. A model for ultrafine powder production in plasma reactor. *Plasma Chemistry Plasma Processing*, 11:371–386, 1991.

[19] J.-F. Bilodeau and P. Proulx. Analysis of ultrafine particle growth in a plasma reactor. *Journal of High Temperature Chemical Process*, 1:141–148, 1992.

[20] A.C. da Cruz and R.J. Munz. Nucleation with simultaneous chemical reaction in the vapor-phase synthesis of aln ultrafine powders. *Aerosol Science and Technology*, 34:499–511, 2001.

[21] A.C. da Cruz. Experimental and modelling study of the plasma vapour-synthesis of ultrafine aluminum nitride powders. PhD thesis, McGill University. 1997, 215 p.

[22] H. Liu. Simulation of a plasma particle generator. MSc thesis, McGill University. 2001, 85 p.

[23] F. Aristizabal. Modelling of the generation of ultra fine aluminum particles from the quech of superheated vapour in turbulent flow. MSc thesis, McGill University. 2002, 157 p.

[24] K.-S. Kim and S.E. Pratsinis. Manufacture of optical waveguide performs by modified chemical vapor deposition. *A.I.Ch.E. Journal*, 34:912–921, 1988.

[25] S.V. Patankar. *Numerical heat Transfer and Fluid Flow.* Hemisphere, New York, 1980, 193 p.

[26] T. Johannessen, S.E. Pratsinis, and H. Livbjerg. Computational fluid-particle dynamics for the flame synthesis of alumina particles. *Chem. Eng. Sci.*, 55:177–191, 2000.

[27] F.W. Kruis, H. Fissan, and A. Peled. Synthesis of nanoparticles in the gas phase for electronic, optical and magnetic applications - a review. *Journal of Aerosol Science*, pages 511–535, 1988.

[28] A. Schild, A. Gutschd, H. Muhlenwg, and S.E. Pratsinis. Simulation of nanoparticle production in premixed aerosol flow reactor by interfacing fluid mechanics and particle dynamics. *Journal of Nanoparticle Research*, 1:305–315, 1999.

[29] G. Rudinger. *Handbook of Powder Technology, vol. 2:Fundamentals of Gas-Particle Flow.* Elsevier, New York, 1980, 142 p.

[30] J.H. Seinfeld. *Atmospheric Chemistry and Physics of Air Pollution.* John Wiley and Sons, New York, 1986, 738 p.

[31] M. I. Boulos and W. H. Gauvin. Powder processing in a plasma jet: A proposed model. *Canadian Journal of Chemical Engineering*, 52:355–363, 1974.

[32] M. Choi. Research in korea on gas phase synthesis and control of nanoparticles. *Journal of Nanoparticle Research*, 3:201–211, 2001.

[33] G.M. Phanse and S.E. Pratsinis. Theory for aerosol generation in laminar flow condensers. *Aerosol Science and Technology*, 11:100–119, 1983.

[34] B.S. MacGibbon, A. A. Busnaina, and B. Fardi. The effect of thermophoresis in particle deposition in a tungsten low pressure chemical vapor deposition reactor. *Journal of the Electrochemical Society*, 146:2901–2905, 1999.

[35] L. Talbot. Thermophoresis, a review. *Rarefied Gas Dynammics*, 74:467, 1981.

[36] J.R. MBrock. On the theory of thermal forces acting on aerosol particles. *Journal of Colloid Science*, 17:768, 1962.

[37] Y.-C. Lee. Modeling work in a thermal plasma processing. PhD thesis, Minnesota University. 1984, 203 p.

[38] S.L. Girshick and C.P. Chiu. Kinetic nucleation theory: A new expression for the rate of homogeneous nucleation from an ideal supersaturated vapor. *Journal of Chemical Physics*, 93:1273–1277, 1990.

[39] R. Becker and W. Dring. *Annals of Physics*, volume 93. 1935, 719-752 p.

[40] N.P. Rao and P.H. McMurry. Nucleation and growth of aerosol in chemically reacting systems. *Aerosol Science and Technology*, 11:120–132, 1989.

[41] R.C. Flagan and J.H. Seinfeld. *Fundamentals of Air Pollution Engineering.* Prentice-Hall, New Jersey, 1988, 542 p.

[42] C. Seigneur, C, A.B. Hudischewskyj, J.H. Seinfeld, K.T. Withby, E.R. Withby, J.R. Brock, and H.M. Barnes. Simulation of aerosol dynamics: A comparative review of mathematical models. *Aerosol Science and Technology*, 5:205–222, 1986.

[43] S. K. Friendlkander. *Smoke, Dust, and Haze: Fundamentals of Aerosol Behaviour.* Wiley, New York, 1977, 432 p.

[44] M. Frenklach and S.J. Harris. Aerosol dynamics using the method of moments. *Journal of Colloid and Interface Sience*, 118:252–261, 1987.

[45] Fluent Incorporated. *Gambit User's Guide.* Version 1.2, 1999.

[46] Fluent Incorporated. *Gambit User's Guide.* Version 5.3.18, 1999.

[47] K.T. Whitby. *The Physical characteristics of sulfur aerosols.* Atmos. Env. 12, 1978, 135-159.